IRAQI JOURNAL OF APPLIED PHYSICS LETTERS

Iraqi Journal of Applied Physics Letters (IJAPLett) is a scientific periodical sponsored and published by the Iraqi Society for Alternative and Renewable Energy Sources and Techniques (I.S.A.R.E.S.T.). The Editorial Board is responsible for the scientific content and other editorial matters relating to the Journal. Manuscripts submitted are first screened by the editors; those on subject matters within the scope of the IJAPLett are sent to an expert referee for evaluation and may be sent to a second reviewer if necessary. This screening process helps to assure an appropriate focus as well as high scientific quality of the Journal. The IJAPLett welcomes submission of papers and letters in applied physics and related fields of science, engineering and technology. They should have something in common with what we now publish on inanimate materials and processes therein: structures, transport, physical, electrical, dielectric, magnetic, and optical properties. Our basic criterion stated below will continue to apply: papers must contain science, especially physics, and there must be an application. We advise authors submitting papers to suggest the names of at least two possible reviewers, with full information on addresses, phone and email. Suggestions of reviewers are welcome regardless of the subject.

EDITORIAL BOARD

Editorial Office
P. O. Box 55259, Baghdad 12001, IRAQ
www.ijap.org, editor@ijap.org
Tel.: 00964 7901274190, Mob.: 00964 7702523071

ADVISORY BOARD

SPONSORED AND PUBLISHED BY

THE IRAQI SOCIETY FOR ALTERNATIVE AND RENEWABLE ENERGY SOURCES AND TECHNIQUES (I.S.A.R.E.S.T.)

PRINTED IN IRAQ **ISSN 1999-656X**

" INSTRUCTIONS TO AUTHORS "

CONTRIBUTIONS

Contributions to be published in this journal should be original research works, i.e., those not already published or submitted for publication elsewhere, individual papers or letters to editor.

SUBMISSION OF MANUSCRIPTS

Manuscripts should be submitted to the editor at the mailing address:

Iraqi Journal of Applied Physics Letters
Editorial Board
P. O. Box 55259, Baghdad 12001, IRAQ
ijaplett@ijap.org , editor@ijap.org

MANUSCRIPTS

Two hard copies with soft copy on a compact disc (CD) should be submitted to Editor in the following configuration:

- Double-spaced one-side A4 size with 2.5 cm margins of all sides
- Times New Roman font (16pt bold for title, 14pt bold for names, 12pt bold for headings, 12pt regular for text)
- Letters should not exceed 10 pages.
- Manuscripts presented in English only are accepted.
- English abstract not exceed 150 words
- 4 keywords (at least) should be maintained on (PACS preferred)
- Author(s) should express all quantities in SI units
- Equations should be written in equation form (*italic* and symbolic)
- Figures and Tables should be separated from text
- Figures and diagrams can be submitted in colors for assessment and they will be returned to authors after provide printable copies
- Charts should be indicated by the software used for
- Only original or high-resolution scanner photos are accepted
- For electronic submission, articles should be formatted with MS-Word software.

AUTHOR NAMES AND AFFILIATIONS

It is IJAPLett policy that all those who have participated significantly in the technical aspects of a paper be recognized as co-authors or cited in the acknowledgments. In the case of a paper with more than one author, correspondence concerning the paper will be sent to the first author unless staff is advised otherwise.
Author name should consist of first name, middle initial, last name. The author affiliation should consist of the following, as applicable, in the order noted:
- Company or college (with department name or company division)
- Postal address
- City, state, zip code, country
- Telephone, and e-mail

REFERENCES

The references should be brought at the end of the article, and numbered in the order of their appearance in the paper. The reference list should be cited in accordance with the following examples:

[1] X. Ning and M.R. Lovell, "On the Sliding Friction Characteristics of Unidirectional Continuous FRP Composites", *ASME J. Tribol.*, 124(1) (2002) 5-13.
[2] M. Barnes, "Stresses in Solenoids", *J. Appl. Phys.*, 48(5) (2001) 2000–2008.
[3] J. Jones, "Contact Mechanics", Cambridge University Press (Cambridge, UK) (2000), Ch.6, p.56.
[4] Y. Lee, S.A. Korpela and R. Horne, "Structure of Multi-Cellular Natural Convection in a Tall Vertical Annulus", Proc. 7th International Heat Transfer Conference, U. Grigul et al., eds., Hemisphere (Washington DC), 2 (1982) 221–226.
[5] M. Hashish, "Waterjet Technology Development", High Pressure Technology, PVP-Vol. 406 (2000), 135-140.
[6] D.W. Watson, "Thermodynamic Analysis", ASME Paper No. 97-GT-288 (1997).
[7] C.Y. Tung, "Evaporative Heat Transfer in the Contact Line of a Mixture", Ph.D. thesis, Rensselaer Polytechnic Institute, Troy, NY (1982).

PROOFS

Authors will receive proofs of papers and are requested to return one corrected hard copy with a WORD copy on a compact disc (CD). New materials inserted in the original text without Editor permission may cause rejection of paper.

COPYRIGHT FORM

Author(s) will be asked to transfer copyrights of the article to the Journal soon after acceptance of it. This will ensure the widest possible dissemination of information.

OFFPRINTS

Authors will receive offprints free of charge and any additional offprints can be ordered.

SUBSCRIPTION AND ORDERS

Annual fees (4 issues per year) of subscription are:

- 50 US$ for individuals inside Iraq.
- 100 US$ for establishments inside Iraq.
- 100 US$ for individuals abroad.
- 200 US$ for establishments abroad.

Fees are reduced by 25% for I.S.A.R.E.S.T. members. Orders of issues can be submitted by contacting the editor-in-chief or editorial office at **subscription@ijap.org** to maintain the address of issue delivery and payment way.

Research Communication

An interesting experimental observation of O_2 pressure effect on the surface roughness of ZnO thin films prepared by PLD technique

Adawiya J. Haider

Professor, School of Applied Sciences, University of Technology, Baghdad, IRAQ, adawiya_haider@yahoo.com

Keywords: *Pulsed laser deposition, ZnO films, Roughness, Oxygen ambient*
Received: 20 October 2009, **Revised**: 3 November 2009, **Accepted**: 7 November 2009

Nowadays, most of the principal optical devices, like light generators, detectors, transmitters, splitters, etc, have been demonstrated. Currently, research is focused on reducing the dimensions of these devices and implementing them as structural elements in integrated optical systems. Hence, new techniques need to be developed for fabricating such systems with dimensions of the individual element down to the micrometer range [1].

ZnO has great advantages for light emitting diodes (LEDs) and laser diodes (LDs) over the currently used semiconductors. Recently, it has been introduced that ZnO as II–VI semiconductor is promising for various technological applications, especially for optoelectronic short wavelength light emitting devices due to its wide and direct band gap. The most important advantage is the high exciton binding energy (60 meV) giving rise to efficient exciton emission at room temperature [2].

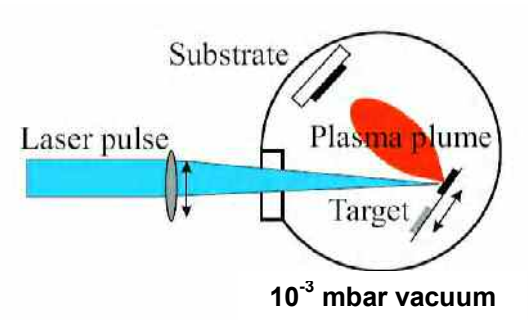

Fig. (1) Schematic diagram of a typical laser deposition set-up

A number of different techniques can be employed for the deposition of oxide materials, including electron beam evaporation (EBV), chemical vapor deposition (CVD), molecular beam epitaxial (MBE), ion-assisted deposition (IAD) and sol-gel methods [3].

Recently, pulsed laser deposition (PLD) proved to be a favorable technique for the deposition of Zinc oxides at different technological conditions on different substrates. That supposed to result in the different structural and micro structural properties and different surface morphology of the nanostructures to be obtained. Also, the optical properties of ZnO are known to be sensitive for its structural quality [4]. PLD offers many advantages compared with other techniques: reduced contamination due to the use of light, control of the composition of deposited structure and in situ doping .The oxygen pressure plays an important role in the film roughness. In this paper, we report the results on the deposition of ZnO thin films obtained at different O_2 pressure by PLD technique. We also investigated the influence of the O_2 pressures on the morphological properties (average Root Mean Square (RMS)) in term of AFM measurements of the films.

Ablation of the target was achieved using an Nd:YAG Second Harmonic Generation (SHG) laser (λ=532nm, pulse duration=7ns and repetition rate of 10Hz). In order to deposit one film, 10min (300 pulses) were applied. We used a set of samples of ZnO purity (99.9999%) and its alloys such as $Mg_xZn_{1-x}O$, $Cd_xZ\ n_{1-x}O$, Al_2O_3, etc). The experimental condition used for our depositions are given in Table (1).

Table (1) Growth parameters

Target	ZnO and its alloys
Substrate	Glass
Substrate-target distance (cm)	4
Fluence (J/cm^2)	1
Substrate temperature (°C)	200
Spot size (mm^2)	0.99
Vacuum pressure(mbar)	10^{-3}
Deposition pressure(O_2) (mbar)	10^{-2}, 10^{-1}, 10
Number of pulses during deposition	300

At 10^{-2}mbar, the surface of the deposited sample appears very smooth and dense, while the others are relatively rough. The average RMS roughness value for the deposited films increased with the O_2 pressure as shown in Fig. (2). The RMS value of the surface at O_2 pressure $5x10^{-2}$ mbar is 50nm. At high O_2 pressure $5x10^{-1}$mbar the surface roughness was found to be 67nm. The roughness is increasing because of the grain formation which can be described as follows. After initial free expansion from the target surface, the mean free path of the ablated particles is reduced in the presence of gas. More specifically, at higher ambient pressure, more collisions and scatterings occur. The particles then lose energy to the level adequate for forming ionic complexes or molecules. If these clusters reach the substrate surface, small grains, start to grow as they become the nucleus. Most of the ablated particles can reach the substrate in the state near the single atoms if the ambient pressure is extremely low. On the other hand, the surface roughness with small grain size is recommended to be as a gas sensitive element [5].

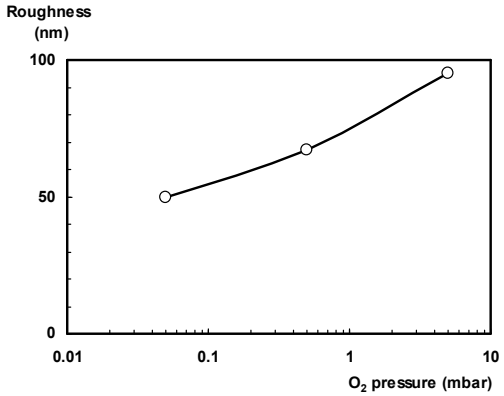

Fig. (2) Dependency of surface roughness of ZnO thin films prepared by PLD on the O_2 pressure inside the deposition chamber

Conclusions

In the foregoing section, we have seen that a high quality semiconductor nanostructure can be fabricated using PLD. A relatively smooth surface and a high crystalline quality, which are appropriate for good optoelectronic devices and applications, were obtained at oxygen pressure of $5x10^{-2}$mbar. But at vacuum of $5x10^{-1}$ mbar, a very low crystalline and a rough surface were obtained. This surface characterization is important for applications in gas sensors and catalysis.

References

[1] C. Phipps, **"Laser Ablation and its Applications"**, Springer (New Mexico, 2007).

[2] L.S. Mende and J.L. MacManus-Driscoll, *Material Today*, 10(5) (2007) 40.

[3] R. Ayouchi et al., "Photosensitivity of Nanocrystalline ZnO Films Grown by PLD", *Appl. Surf. Sci.*, article in press (2009).

[4] R. Khandelwal et al., *Opt. Laser Technol.*, 40 (2008) 247.

[5] T. Mazingue et al., *Appl. Opt.*, 45 (2006) 1425.

2010 INTERNATIONAL CONFERENCE ON COMPOUND SEMICONDUCTOR MANUFACTURING TECHNOLOGY

May 17th - 20st, 2010

Marriott – Waterfront, Portland, Oregon, USA

CALL FOR PAPERS

Come to the 25th **CS MANTECH** in May 2010! To celebrate this anniversary, there will be some special sessions looking back at our progress and ahead to the future.

Our focus is optimum manufacturing practices for all compound semiconductor (CS) device technologies - the practical "nuts and bolts" of CS device production including design, materials, fabrication, and test.

We welcome submissions about all CS technologies. **Students are particularly encouraged to submit abstracts.** The program includes practical ***Technical Sessions*** including ***Invited Papers*** presented by technologists from around the world on a variety of topics, an intensive multi-topic ***Workshop***, and an ***Exhibit*** featuring leading equipment, supply, substrate, epitaxy, and process chemical vendors and special service providers. ***Events*** like the ***Exhibits Reception***, the ***International Reception***, the ***Interactive Forum***, and informal ***Rump Sessions*** provide opportunities to network and develop business contacts. And in 2010, for the first time, the ***ROCS Workshop*** will be held at Mantech.

Manufacturing-Related Papers Solicited

Our mission is to foster the growth and success of the CS industry by encouraging the sharing of best manufacturing technologies and practices among peers in an open, informal environment. *Manufacturing technologies of interest include those for GaAs, InP, GaN and other nitrides, SiC, Diamond, Sb compounds, SiGe, and other related materials.* Papers addressing manufacturing challenges are sought in, but not limited to, the following subject areas:

MANUFACTURING

- Fab Optimization
- Foundry Operations
- Technology Transfers
- Cycle-Time Reduction
- Production Modeling
- Design Strategies
- Quality and Training
- Tool Selection
- Environmental Impact
- Yield & SPC

PROCESSING/ CONTROL

- Lithography
- Etch & Etch Stops
- Gate Formation
- Metrology
- Novel Control Techniques
- Backend and Backside
- Thin Films & Metallization
- Multi-Level Interconnects

RF DEVICE TECHNOLOGIES:

- MESFET, HFET, HEMT
- PHEMT, MHEMT
- HBT, PIN, MEMS
- Performance & Yield
- Process Simplification
- Heterogeneous Integration
- Device Tech Integration
- Integrated Passives

TEST & RELIABILITY

- High Volume/ Low Cost
- In-Process
- Test Structures
- On-Chip Self Test
- Failure Modes/ Analysis
- Fault Identification
- Reliability Testing
- ESD

OPTICAL DEVICES & CIRCUITS

- LEDs, VCSELs
- Lasers, OEICs
- Modulators & Detectors
- Waveguides
- Lighting Technologies
- Process Simplification
- Fabrication Control
- Process & Circuit Integration

EMERGING AND COMPETING TECHNOLOGIES

- Wide Bandgap
- Narrow Bandgap
- InP, SiGe, Strained Si
- Plasma Wave Devices
- Si CMOS, LDMOS
- New Technologies

MATERIALS

- Availability & Quality
- Standards
- Cost Reduction
- Recycling
- Epitaxy
- Metamorphic Material

PACKAGING

- High Frequency
- Bump and Flip Chip
- System in Package
- Hermeticity & Reliability
- Thermal Management
- Photonic Packaging
- 3-D Packaging & Pb-Free MSL

FUTURE

- Technology Roadmap
- Business Outlook
- "Killer" Applications
- New Paradigms

ABSTRACTS DUE NOVEMBER 18, 2009

Send a 1- or 2-page abstract in PDF or WORD format to *abstracts@csmantech.org*

Please use U.S. fonts only.

Look for abstract guidelines at www.csmantech.org

Conference Chair
Steve Mahon
smahon@tqs.com

Technical Program Chair
Yohei Otoki
otoki@hitachi-cable.com

Registration Chair
Alex Smith
asmith@brewerscience.com

Exhibits Chair
Paul Cooke
pcooke@iqep.com

Publicity Chair
Nick Kolarich
nick_kolarich@kopin.com

University Liaison
Mariam Sedaka
mariam.sedaka@gmail.com

Abstracts should clearly state:

- The ***Purpose*** of the work.
- How CS ***Manufacturing Technology*** was advanced or how a competing technology relates to CS devices.
- What ***Specific Results*** were obtained? Supporting data, charts and pictures are requested.

All abstracts should include keywords to facilitate indexing for classification and search in our database. Papers describing related work performed in university or government centers should clearly describe the application to manufacturing. ***Student Papers*** should be clearly identified as such. An annual prize is given for the best student paper presented at the conference.

Note: Large files over 1 MB in size may not transmit successfully. Please use self-extracting or "zip" files to facilitate transmission of such large files.

Notice of paper acceptance will be e-mailed no later than **December 15, 2009**. Authors of accepted papers must submit a publication-ready extended abstract by **February 9, 2010**. The extended abstracts will be published in the MANTECH Conference Digest and will become the property of GaAs MANTECH, Inc. It is the author's responsibility to obtain any required clearance prior to submission of both the abstract and the extended abstract.

Students and University researchers seeking financial assistance to attend the Conference should contact Scott Davis at student.aid@csmantech.org.

ABSTRACTS DUE NOVEMBER 18, 2009

Send a 1- or 2-page abstract in PDF or WORD format to *abstracts@csmantech.org* .
Please use U.S. fonts only.

Look for abstract guidelines at www.csmantech.org

Portland, Oregon

Portland, the City of Roses, is a great place to get away from your busy, stressful life. Besides the historic oldtown area, there are numerous galleries, museums, and a wide variety of parks and green areas. Plus the famous Willamette Valley wineries are only a short drive away. It's also good to know that Oregon has no sales tax, so Portland is a great place for shopping.

Don't miss this opportunity to visit Portland, and attend ManTech 2010!

Analytical Determination of Coherence Coefficient of Uniform-Distributed Wave Propagation

Noor E.N. Alrawi

School of Applied Sciences, University of Technology, Baghdad, Iraq

In this work, we have derived an analytical expression for the mode-coherence coefficients of uniform-distributed wave propagating within different media as in case of hyperbolic Gaussian beams, as well as proposed a simple method of superposition of two such beams. Such obtained results are extremely useful to study and analyze the propagation of Hermite-Gaussian beams especially in the problems of radiation interaction with matter and laser beam propagation concerned in modern free-space and fiber optical communications.

Keywords: *Wave propagation, Coherence coefficient, Uniform-distributed waves, Gaussian beams*
Received: 6 August 2009, **Revised**: 25 September 2009, **Accepted**: 2 October 2009

1. Introduction

With the decreasing availability of RF spectrum and the increasing demand for higher communications bandwidths, the terahertz laser communications bandwidths are seen as a viable augmentation of RF communications capability. Yet, cloud cover effects can impact link availability. Among the key strategies to increase availability and mitigate cloud cover effects is the global deployment of ground stations in atmospherically independent cells. Yet with such a deployment, one needs to address the impact of the uplink laser beams (the power densities on the communications downlink are usually eye safe) on the flying public and on space assets sensitive to laser radiation. Although the power densities of the uplink beacon required for Earth orbiters to track the ground station can, depending on mission, be within eye-safe laser levels, this will not be so when operations call for transmitting a beacon or commands to deep-space probes [1].

The discovery of propagation-invariant beams naturally led to the idea of similar pulses or wave packets. Solitons are, of course, well-known for waves propagating in nonlinear media where the nonlinearity serves to counterbalance the effect of diffraction. Similarly (radial) changes in the index of refraction can be used to form a waveguide that supports localized waves. In free space or in a linear medium, no such equities are available. Periodically propagating waves are not strictly propagation-invariant although they avoid diffractive spreading by returning to their original pattern after a certain propagation distance or time. They are further allowed to rotate in-between. A systematic approach has been introduced for all periodically evolving pulsed waves for velocities $0<v<\infty$. Their spectral characteristics vary according to whether this velocity of propagation equals, exceeds, or is below the speed of light.

Casperson *et al.* has presented a novel type of beam, Hermite–sinusiodal-Gaussian beam [2-4]. Among the family of Hermite–sinusiodal-Gaussian beams, the cosh-Gaussian beams are of much interest, because their beam profiles are suitable for practical applications [2,4]. On the other hand, it was shown by Siegman [5,6], Weber [7] and Du *et al.* [8,9] that the beam-propagation factor (M^2 factor) and the mode coherence coefficients are very useful beam parameters for characterizing various laser beams and their mode structures. In this letter, we study the beam-propagation factor and the mode coherence coefficients of cosh-Gaussian beams, as well as to propose a simple method for producing cosh-Gaussian beams experimentally.

ISSN 1999-656X PRINTED IN IRAQ

2. Analysis

The field distribution $E(x,z)$ of two-dimensional cosh-Gaussian beams at the plane z=0 is characterized by [4]

$$E(x,0)=\exp\left(-\frac{x^2}{\omega_0^2}\right)\cosh\left(\Omega_0 x\right) \tag{1}$$

where ω_0 is the waist width of the Gaussian amplitude distribution, Ω_0 is the normalized parameter of cosh-Gaussian beams, and cosh denotes the hyperbolic cosine function, which can be written as

$$\cosh(\theta)=\frac{e^{\theta}+e^{-\theta}}{2} \tag{2}$$

Substituting Eq. (2) into Eq. (1) yields

$$E(x,0)=\frac{\exp\left(\frac{\omega_0^2\Omega_0^2}{4}\right)}{2}\left(e^{-a}+e^{-b}\right) \tag{3}$$

where

$$a=\frac{x-\frac{\omega_0^2\Omega_0^2}{2}}{\omega_0^2};\qquad b=\frac{x+\frac{\omega_0^2\Omega_0^2}{2}}{\omega_0^2}$$

An alternative interpretation of Eq. (3) is that a cosh-Gaussian beam can be regarded as a superposition of two Gaussian beams with the same waist width and in phase, whose centers are located at ($\omega_0^2\Omega_0/2$,0) and (-$\omega_0^2\Omega_0/2$,0) in the xz plane. Thus, cosh-Gaussian beams can be simply realized experimentally by superposition of two decentered Gaussian beams. Furthermore, the most-general complex form of HSG mode can be obtained by superposition of two of the generalized Hermite–Gaussian beams [2]. The intensity distribution of cosh-Gaussian beams at the z=0 plane reads as

$$I(x,0)=E(x,0)E^{*}(x,0) \tag{4}$$

with * denoting the complex conjugate.

In accordance with the second-moments definition of the variance σ_x^2 in the spatial domain and the variance σ_k^2 in the spatial-frequency domain [4], after performing the standard integral procedures (e.g., Refs. 4 and 6) with Eqs. (3) and (4) taken into account, we have

$$\sigma_x^2=\frac{\omega_0^2}{4}\left[1+\frac{\delta}{1+\exp\left(-\frac{\delta}{2}\right)}\right] \tag{5}$$

$$\sigma_k^2=\frac{1}{4\pi^2\omega_0^2}\left[1+\frac{\delta\exp\left(-\frac{\delta}{2}\right)}{1+\exp\left(-\frac{\delta}{2}\right)}\right] \tag{6}$$

Where

$$\delta=\omega_0^2\Omega_0^2 \tag{7}$$

Therefore the M^2 factor of the cosh-Gaussian beams is obtained readily from Eqs. (5) and (6) and is given by

$$M^2=4\pi\sigma_x\sigma_k \tag{8a}$$

$$M^2=\frac{\sqrt{(1-\delta)e^{-\delta}+\left(2-\delta^2\right)e^{-\frac{\delta}{2}}+\delta+1}}{1+e^{-\frac{\delta}{2}}} \tag{8b}$$

3. Results and Discussion

Equation (8) indicates that the M^2 factor of the cosh-Gaussian beams depends only on $\delta=\omega_0^2\Omega_0^2$. Figure (1) gives the variation of the M^2 factor of a cosh-Gaussian beam versus d, from which it turns out that the M^2 factor of the cosh-Gaussian beam decreases with $\delta(\delta\geq 0)$ monotonically. In addition, $M^2\geq 1$ and reaches the minimum value 1 if δ=0 (i.e., Ω_0=0) in the limiting case of the Gaussian beam.

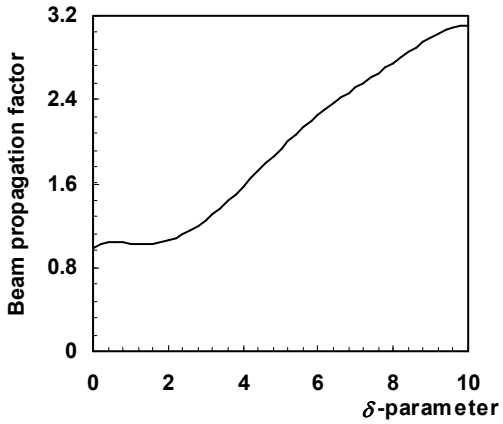

Fig. (1) Beam propagation factor (M^2) factor of a hyperbolic Gaussian beam as a function of δ

It is well known that the field distribution $E(x,z)$ of light at the plane of z=0 can be expanded into a series of orthogonal basis modes $\varphi_m(x)$, i.e.,

$$E(x,0)=\sum_m c_m\varphi_m(x) \tag{9}$$

where c_m denotes the mode coefficients, m the mode indices, and $\varphi_m(x)$ the series of orthogonal basis modes, for example, the Hermite-Gaussian modes of the form

$$\varphi_m(x)=U_m\exp\left(-\frac{\alpha^2x^2}{2}\right)H_m(\alpha x) \tag{10}$$

where U_m is the normalized factor, a is related to the waist width ω_{0h} of the basis Gaussian mode by

$$\alpha=\frac{\sqrt{2}}{\omega_{0h}} \tag{11}$$

and the unimportant phase factor is omitted in Eq. (10) for the sake of convenience.

Substituting Eq. (1) into Eq. (9), and using the orthogonality of the Hermite-Gaussian series, we have

$$c_m = \int_{-\infty}^{+\infty} \varphi_m^*(x) e^{-\frac{x^2}{\omega_0^2}} \cosh(\Omega_0 x) dx \qquad (12)$$

The direct combination of equations. (10) and (12) leads to

$$c_m = \sqrt{\frac{\sqrt{\pi}v}{\alpha(2+v)}} \exp\left(\frac{\delta}{2(1+v)}\right)\left(\frac{2-v}{4+2v}\right)^{\frac{m}{2}} \frac{1}{\sqrt{m!}} H_m\left(\frac{v\delta}{\sqrt{4-v^2}}\right) \qquad m = even \qquad (13)$$

Otherwise, c_m=0 when m is odd, where

$$v=\omega_0^2\alpha_0^2 \qquad (14)$$

Equation (13) implies that cosh-Gaussian beams contain only even Hermite-Gaussian modes. Figure (2) shows the analytical relation of the mode coefficient (c_m) to the mode index (m) within the examined values of beam propagation factor.

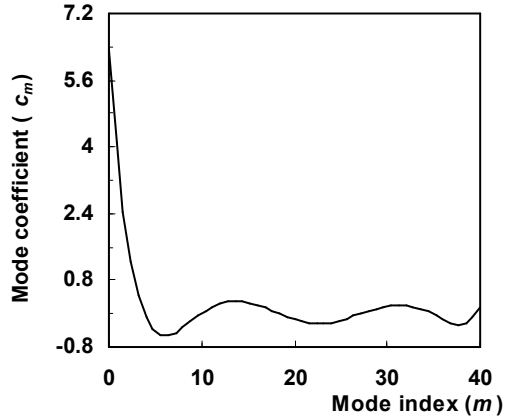

Figure (2) shows the analytical relation of the mode coefficient (c_m) to the mode index (m) within the examined values of beam propagation factor.

4. Conclusion

Simple method has been proposed by which hyperbolic Gaussian beams can be realized experimentally without the use of a sophisticated aperture. Both the M^2 factor and the mode coherence coefficients of hyperbolic Gaussian beams have been expressed in the closed form, which is suitable for use in applications and provides a comprehensive characterization of hyperbolic Gaussian beam qualities such as beam invariance, beam quality, mode structure, and correlation. Finally, it should be stressed that here the hyperbolic Gaussian beams have been taken only as an illustrative example. The above approach and results have more generally applicable advantages and can be used to study three-dimensional hyperbolic Gaussian beams those can be produced experimentally by superposition of two decentered Gaussian beams with the same width but π dephase.

References

[1]K.E. Wilson et al., "Plan for Safe Laser Beam Propagation from the Optical Communications Telescope Laboratory", IPN Progress Report 42-152, February 15, 2003.
[2]L.W. Casperson, D.G. Hall, and A. A. Tovar, *J. Opt. Soc. Amer.,* A14 (1997) 3341.
[3]L.W. Casperson and A. A. Tovar, *J. Opt. Soc. Amer.*, A15 (1998) 954.
[4]A.A. Tovar and L. W. Casperson, *J. Opt. Soc. Amer.,* A15 (1998) 2425.
[5]E. Siegman, *Proc. SPIE,* 1224 (1990) 2.
[6]E. Siegman, in DPSS *Lasers: Application and Issues*, M.W. Dowley, ed., Vol. 17 of OSA Trends in Optics and Photonics Series (Optical Society of America, Washington, D.C., 1998), p. 184.
[7]H. Weber, *Opt. Quantum Electron.,* 24 (1992) 1047.
[8]K.M. Du, G. Herziger, P. Loosen, and F. Rühl, *Opt. Quantum Electron.*, 24 (1992) 1081.
[9]A. Starikov and E. Wolf, *J. Opt. Soc. Amer.*, A72 (1982) 923.

IRAQI JOURNAL OF APPLIED PHYSICS

Found in 2005, Find in 2009

By
Oday A. Hamadi
Managing Editor, IJAP

ENDING EVERY YEAR, the Editorial Board of IJAP works hard to diagnose and study its progress and interaction with the scientific research community in Iraq throughout collecting and analyzing the statistic data both quantitatively and qualitatively, as well as throughout the direct opinions extracted from samples based on time and field variety inside the scientific research community in Iraq. In this issue, the last of 2009 volume, we will preview the classification of the articles published in IJAP since its first issue in January 2005 ending with this current issue according to the nine branches of applied physics dedicated by IJAP. Also, we will preview the classification of authors of these articles as Iraqis, Arabs or Foreign. We think that both classifications may assist IJAP to proceed into the horizon of development and growth during the next years.

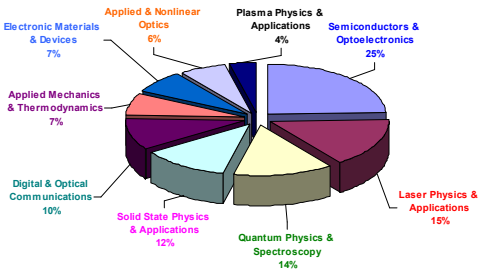

Articles published in IJAP (2005-2009) by subject

This study explains that about 25% of the published article were on *semiconductors & optoelectronics*, whereas 15% on *laser physics & applications*, 14% on *quantum physics & spectroscopy*, 12% on *solid state physics & applications*, 10% on *digital & optical communications*, 7% on *applied mechanics & thermodynamics*, 7% on *electronic materials & devices*, 6% on *applied & nonlinear optics* and 4% on *plasma physics & applications*. As well, this study explains that about 73% of authors were *Iraqis*, 25% *Foreign* and only 2% *Arabs*.

Accordingly, we can highlight some points from this analysis. The reality of scientific research in Iraq allowed Iraqi researchers – either individuals or groups – to work on *semiconductors & optoelectronics* much more than other fields. They work on solar cells, photodetectors, deposition and doping techniques (such as LID, PLD, CVD, PECVD, CBD, spray pyrolysis, etc.), crystal growth, production of nanostructures, optical and electrical properties of thin films, thermal annealing and photoconductivity. This may be attributed to the open technology, clearness of theories, availability of competed experts – either from foreign or national universities – and lower financial and technical requirements when compared to other fields.

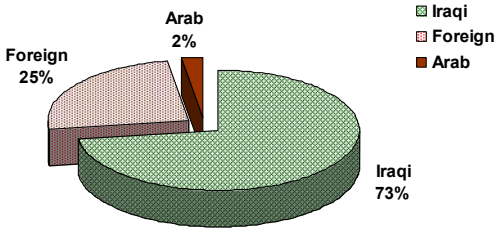

Authors of IJAP articles by nationality

The fields of high financial and technical requirements, such as *plasma physics & applications*, *applied & nonlinear optics*, *electronic materials & devices*, and *applied mechanics & thermodynamics*, have found less interest by Iraqi authors those published their articles in IJAP and most of the published articles in such fields were submitted by foreign authors. Most articles on *digital & optical communications*, *solid state physics & applications*, and *quantum physics & spectroscopy*, submitted by Iraqi authors, were dealing with simulation and modeling works, while the articles on *laser physics & applications* submitted by Iraqi authors have combined between experimental and theoretical works, however, such theoretical studies have based upon experimental results. This highlights the availability of good Iraqi experiences on laser physics and applications within the available possibilities and resources.

This study highlights that 50% of the published articles were on *semiconductors & optoelectronics*, *laser physics & applications*, and *digital & optical communications*, as the results and outcomes of these branches can applicably and directly be found over the academic and research fields as well as the daily life of the modern society.

Despite the acceptable echo of IJAP inside the scientific research community in Iraq and the interesting contributions from foreign authors, which represent a "record" over Iraqi and Arab scientific journals, the Arabic contributions still small. This is attributed mainly to the electronic distribution style considered by IJAP rather than the printed hard copies, which in turn due to the poor financial resources of IJAP. Otherwise, IJAP hard copies may be available in too many libraries in Arab universities. As well, the scientific research communities in Arab countries do not respond to Arabic scientific journals and periodicals as required that makes IJAP a new experiment among the Arab specialized scientific journals.

Bulk Solid Specimen Shape Dependences in the Molecular, Chemical-Shift Tensor Determinations

S. Aravamudhan

Department of Chemistry, North Eastern Hill University, Shillong 793022 Meghalaya, India

In this paper, it has been the effort to systematically document the salient results of the calculations which are taking the course from molecule to material. The ellipsoidal shapes are the ones which have the homogeneous magnetization for homogeneous susceptibility. The computer programs used in this analysis were written FORTRAN. Moreover, a simpler summation procedure could be evolved for the calculation of the shape dependent demagnetization factor.

Keywords: *Shape dependences, Molecular solid, Chemical-shift tensor, Homogeneous susceptibility*
Received: 6 August 2009, **Revised**: 25 September 2009, **Accepted**: 2 October 2009

1. Introduction

In diamagnetic molecules the electrons, which are all spin-paired, undergo circulatory motions centered on the atomic nuclei in the molecular frame-work. In the case of diamagnetic molecular systems, there are two electrons in each of the occupied molecular orbital. The occupancies in molecular orbitals entails the possibility that the charge circulations of the electrons in the orbitals can be in the opposite directions. Thus even though there are continuous circulations of electrons there can be cancellations of the induced fields because of the circulations in opposite directions. When an external magnetic field is applied, there can be preferences established for circulations in one direction over the other alternative direction and there could be changes in the velocity of circulations and the circulation paths. Such effects in the environment of bonded atoms can have varying effects significant enough to indicate the electronic structures. It is primarily these differences in induced fields which are of interest to chemists while investigating spectroscopically, and, in particular using the NMR Spectroscopic tool.

The situation described above, for a diamagnetic molecule, is entirely with respect to the intra molecular perspectives for induced fields at the site of nuclei. What compounds this description of induced field at particular site is the fact that there are contributions to induced fields from other molecules. There are molecules which are in the immediate vicinity as well as from the distant locations in a continuous distribution over the entire macroscopic extent of the specimen, which at any particular instance, can be a single crystal of organic molecule. Under the influence of external magnetic field the electronic circulations prevailing are the same in every one of the independently identifiable equivalent molecules which are present in the crystal. The induced fields due to a molecule at a given site differ depending upon whether that specified site is occupied by a proton bonded to that molecule or in any molecule located in any of the other the lattice sites.

It is a fact that the induced fields arising at a site, due to the specified repeating-unit of the electronic structure in the lattice (which is a molecule in the particular case), must be considered always inseparably with the induced fields from the other lattice site units. This makes the estimation of induced fields for a given site to become complicated and laborious to evaluate. While approximations are resorted to, then the uncertainties in the calculated estimates in conjunction with the accuracies of experimental measurements render the interpretations to be less conclusive.

Determination of the chemical shift tensors (measured with respect to a 'reference' chemical-compound) requires using single crystals of organic molecules and these are diamagnetic specimen. The chemical shifts arise due to variations in induced fields at a proton (nuclear) site within a molecule, due to the changes in the

ISSN 1999-656X PRINTED IN IRAQ

electron charge circulations within the molecules when placed in a strong external magnetic field. The solid-state High Resolution Proton Magnetic Resonance (HR PMR) techniques yield tensor values measured experimentally, but it becomes necessary to calculate and take into consideration the intermolecular contributions to the chemical shifts to retrieve the only 'intra molecular' shift tensor values. The intermolecular contributions in principle can be contribution beginning from the molecule which is immediate neighbor and the other molecules which are distant neighbors extending to the entire extent of the macroscopic specimen. Thus it raises the questions pertinent for taking into consideration the induced fields from the entire bulk of the specimen at a point within the specimen which typically are the issues in the study of magnetic materials. Seeking answers to such questions as is necessary to validate the procedures used for the retrieval of the intra molecular values as mentioned above. These questions and, the answers seem to pave the way to secure certain clarifications pertaining to field distributions within magnetized materials. Thus evolving a criterion to correct for the bulk specimen shape dependences in the context of the measurement of proton Chemical Shift Tensor paves the way to unravel the consequences of induced field distributions within the material medium. This path-way, from molecule to materials, seem to be refreshing the understanding of the requirements laid out for the specifications of local fields at points within a specimen with bulk magnetization features.

2. HR PMR Experiments

The High Resolution Proton Magnetic Resonance (HR PMR) experiments in Solids have been well described in the literature [1]. It is reiterated here that the single specimen used for the measurements in HR PMR in solids have been spherically shaped; for reasons that the bulk susceptibility contribution to induced fields within the specimen is zero for the spherical shape of the specimen. This limits the utility of this technique since it is not always possible that the given organic molecular single crystal can be shaped into a sphere for the convenient use for measurement by HR PMR techniques. The current experimental efforts are being made to reduce the experimental constraints in making spheres.

3. Perspectives for Considerations of the Specimen Consequentially as Material

The considerations which are also pertinent to consequences in magnetic material begin with this effort by which the intermolecular contributions were calculated by rigid lattice summation procedures.

Experimental determination of Shift tensors by HR PMR techniques in single crystalline solid state, require Spherically Shaped Specimen. The bulk susceptibility contributions to induced fields is zero inside spherically shaped specimen. The above criterion requires that a semi micro spherical volume element is carved out around the site within the specimen and around the specified site this carved out region is a cavity which is called the Lorentz Cavity. Provided the Lorentz cavity is spherical and the outer specimen shape is also spherical, then the criterion 1 is valid. In actuality the carving out of a cavity is only hypothetical and the carved out portion contains the atoms/molecules at the lattice sites in this region as well. The distinction made by this hypothetical boundary is that all the materials outside the boundary is treated as a continuum. For matters of induced field contributions the materials inside the Lorentz sphere must be considered as making discrete contributions.

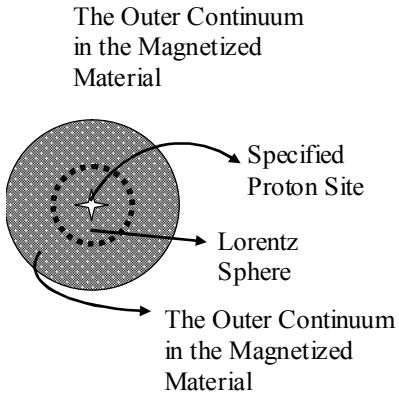

Fig. (1) The hypothetical division of the spherical sample for consideration from the perspectives of a material medium

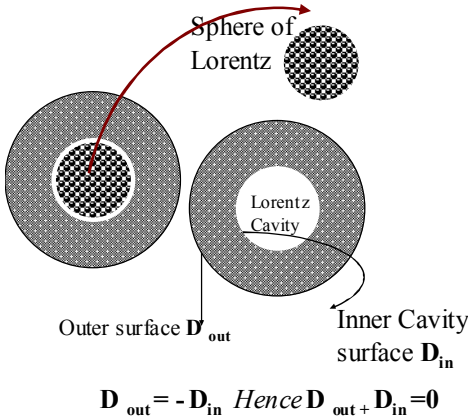

$$\mathbf{D}_{out} = -\mathbf{D}_{in} \quad Hence \quad \mathbf{D}_{out} + \mathbf{D}_{in} = 0$$

Fig. (2) Explaining the consequence of zero induced field inside the spherical specimen. The D with subscripts stand for the demagnetization factors of the corresponding boundary surfaces-inner & outer

Equation for calculation of Shielding (induced field) by discrete summation of the

contributions from within the Lorentz sphere. Explicit expression in terms of the matrix indicating the required matrix multiplication steps for such calculation

$$\sigma_T = \left[\frac{X_T}{R_v^3} - \frac{3[R_v R_v]_T X_T}{R_v^5} \right] \quad (1)$$

where σ_T is shielding terrace, $R_v = i_0 x + j_0 y + k_0 z$ is rational vector from nuclear site to the point dipole, and X_T is susceptibility terrace

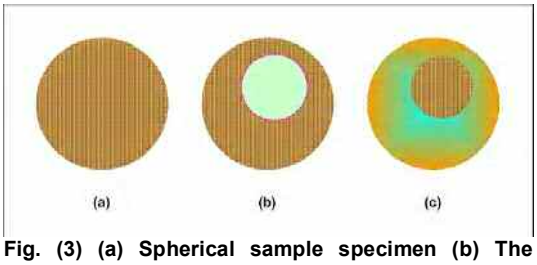

Fig. (3) (a) Spherical sample specimen (b) The Lorentz spherical cavity (c) & The Lorentz sphere in place as discrete region, within the extent of continuum

Equation (1) is used to calculate the discrete sum over the lattice points within the Lorentz sphere.

4. The Ellipsoidal Semi Micro Volume Elements Instead of Spheres for the Discrete Summation

The sections (4) and (5) of Ref. [1] contain the discussions for this aspect. It has been argued out that as much as there is reason for induced field to be zero within the magnetized spherical specimen, there is equally a valid argument as to why the induced fields within an ellipsoidal specimen also can be zero. However, this point of view has till now not been brought forward and it is in the context of intermolecular contributions in HR PMR in solids the ground could be laid for these reasons to be brought to stay. To gain better insight into the arguments and reasons for prevailing practices it became necessary to investigate the trends and final limiting values for convergence of the sum of contributions within the semi micro ellipsoidal volume elements. Such calculations indicate that even if during the summation the summed values are different for spheres and ellipsoids after a critical value for the spherical radius and the major axis length value for the ellipsoids the limiting values are the same. Which means for the sphere the value being zero for cubic lattice for the ellipsoidal element also the sum goes to zero after a certain size of the ellipsoid and for several values of ellipticities indicating that ellipsoidal elements for all constants and types of lattices, can be replaced by a an effectively spherical volume element. That shape dependent factor which is supposed to be the value of such a summation over the entire set of lattice points in the macroscopic specimen seems inexplicable from this result that the discrete summation results in the same sum total value for induced field contribution within sphere and ellipsoids of any shape factor (ellipticity). Thus why does the demagnetization factor different? Only because outer shape and inner shapes are different? Even this can be argued that the inner contribution not being dependent upon shape can be replaced with any shape that the macroscopic specimen has and the dimensions being of semi micro ranges.

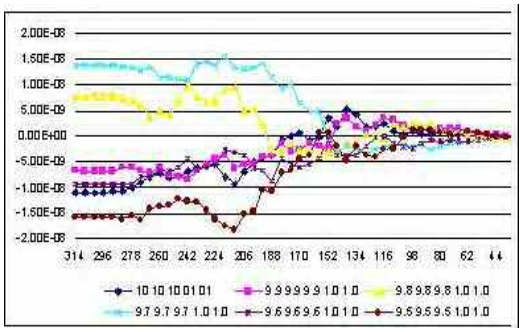

Fig. (4) A graphical display of the trends of summed values as a function of the radius in angstrom units from the proton site. Isotropic susceptibility is used. Cubic lattice with varying lattice constants indicated by the difference in the color of lines. Horizontal axis is increasing (from right to left) radius of sphere. All values on Y-axis are of the order of 10^{-8} or less. This order of magnitude seems to be taken as zero for practical considerations

In such an event a certain trends indicated that the contributions from inside the semi micro volume element seem to dominate in value over the entire contribution from the remaining bulk of the specimen by several orders of magnitude that, the importance of macroscopic shape is relative and the demagnetization factor is only a multiplicative factor for the shape and when the multiplied value is less in magnitude than the semi micro volume element contribution, the dependences on shape factors may not be important for practical purposes for the induced field values at any particular site within the macroscopic specimen. Since this is all the arguments for diamagnetic specimen, similar calculations for paramagnetic and other magnetic materials seem warranted and in the presentation this point of view would be emphasized and highlighted. Thus from the above graphical plot it seems it is obvious that the sum of contributions of induced field at the centre of a sphere is zero for typical variety of cubic lattice constants.

It is possible to compare the situation for inner sphere (semi micro) and the inner ellipsoid the remaining factors remaining the same. Figure (5) to follow contains the results for summing for non-cubic lattice and the inner semi micro element for discrete summation is a sphere. The

y-axis values range from 10^{-8} to 10^{-3} as in the previous case and the different lines for different lattice constants. This can be provided a comparison with an inner ellipsoid.

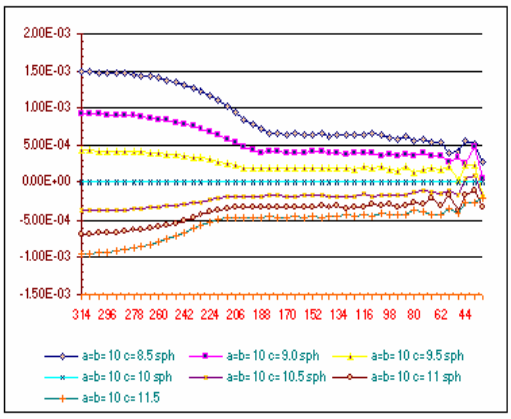

Fig. (5) INNER Element is Spherical and Convergence trends are indicated. The Pink Line corresponds to the case of a=b=10 c=9.0 Spherical inner element radius increases from 44 to 314Å. As the 'C' axis lattice constant value changes from 8.5 to 11.5Å, The convergence value gradually decreases [through 'zero' for cubic case] to negative

It has been the effort to systematically document the salient results of the calculations which are taking the course from molecule to material. The ellipsoidal shapes are the ones which have the homogeneous magnetization for homogeneous susceptibility. Hence the case of inhomogeneity is yet to be discussed. More over when it is of importance to consider point by point summed contribution within the inner sphere, it must be obvious that even in the case of the favourable zero induced filed cases, the sum total of the discrete summation varies significantly from one point to other. If this summed value is significant compared to the bulk continuum contribution, then the assertion that the magnetization is homogeneous for spherical & ellipsoidal specimen would have to be reconsidered and ensure that it is only an average [2] picture which is being refereed which includes averaging the discrete summing of point to point. This being so for diamagnetic specimen what would be the criteria set for magnetic materials where the internal fields are large? These points would be enumerated while presenting the material.

5. Conclusions

The references cited here are mainly for the documentations made for the calculations made by this author. More references of much earlier efforts to handle internal field values at specific sites would also be referred and yet another version of this manuscript would become due after the presentation. A simpler summation procedure could be evolved for the calculation of the shape dependent demagnetization factor.

Refrences

[1] S. Aravamudhan, *Indian J. Phys.*, 79(9) (2005) 985-989.

[2] (a) D.E. Aspnes, Local-field Effects and Effective-medium theory: A Microscopic perspective, *Amer. J. Phys.*, 50(8) (1982) 704-708 (b) S.E. Schnatterly and C. Tario, Local Fields in Solids: microscopic aspects of dielectrics, *Rev. of Modern Phys.*, 64 (1992) 619-622.

A Novel Multiband and Small Size Patch Microstrip Fractal Antenna for Wireless Applications

Fawwaz J. Jibrael [1]
Mahir H. Hammed [2]

[1]*Department of Electrical and Electronic Engineering, University of Technology, Baghdad, Iraq*
[2]*Department of Electrical and Electronic Engineering, Al-Mustanssyriah University, Baghdad, Iraq*

A novel compact Plusses fractal patch microstrip antenna is investigated to be an efficient scheme of miniaturization based on the simulation results, the proposed antenna has shown to possess an excellent size reduction possibility with good radiation performance for wireless applications. The new designed antenna has an operating frequency of 2.46 GHz, 6.58 GHz, and 9.2 GHz, with acceptable bandwidth and S_{11}≤-10 dB (VSWR≤2). The radiation characteristics, VSWR, and S_{11} of the proposed antenna are described and simulated using microwave office MWO 2007 v7.5.

Keywords: *Patch antenna, Microstrip antenna, Fractal antenna, Multiband antenna*
Received: 20 July 2009, **Revised**: 24 October 2009, **Accepted**: 1 November 2009

1. Introduction

A fractal is recursively generated object having a fractional dimension. The term fractal, which means broken or irregular fragments, was originally coined by Mandelbrot [1] to describe a family of complex shapes that possess an inherent self-similarity in their geometrical structures. Since then, a wide variety of applications for fractal has been found in many areas of science and engineering. One such area is fractal electrodynamics [2,3], in which fractal geometry is combined with electromagnetic theory for the purpose of investigating a new class of radiation, propagation, and scattering problems. One of the most promising areas of fractal electrodynamics research is its application to the antenna theory and design.

Another prominent benefit that has been derived from using fractal geometries in antenna has been to design for multiple resonances [3,4]. Fractals are complex geometric shapes that repeat themselves, and are thus self similar. Because of the self-similarity of the geometry due to the iterative generating process, the multiple scales of the recurring geometry resonate at different frequency bands.

Fractals represent a class of geometry with very unique properties that can be attractive for antenna designers. Fractal space filling contours, meaning electrically large features can be efficiently packed into small area .Since the electrical lengths play such an important role in antenna design, this efficient packing can be used as viable miniaturization technique. The space filling properties lead to curves that are electrically very long, but fit into a compact physical space. This property can lead to the miniaturization of antenna elements.

Microstrip antennas offer many advantages such as low profile, the ease of fabrication, and the low cost. These make them very popular and attractive for the designers since the early days they appear. In many cases, where the antenna size is considered an important limitation, their large physical size, make them improper to be used in many applications. Several methods have been considered to reduce the antenna size such as the use of shorting posts [5], material loading and geometry optimization [6]. Use of slots with different shapes in patch microstrip antennas had proved to be satisfactory in producing miniaturized elements [7-9]. Recently more research works have been devoted to make use of the space-filling property of some fractal objects to produce miniaturized antenna elements [10].

In this paper, A multiband and small size antenna is presented as a candidate for use in applications such as wireless local area network (WLAN system of IEEE 802.11b standard-2.4GHz.), industrial scientific medical (ISM-2.4GHz.), and Bluetooth frequency of 2.45GHz.

2. Generation of the Plusses Fractal Antenna

Fractals are basically geometric figures created from a very simple pattern that becomes more complex as we repeatedly apply a certain rule. In many cases, the rule changes the original figure by adding or removing portions of the figure. This process is repeated an infinite number of times. One of the simplest fractals to visualize and work with mathematically is the Plusses fractal. Start with a + sign and add plus signs that are half the size to each of the four line ends. Figure (1) shows how the Plusses fractal grows after 3 iterations. Notice how the + sign grows into the shape of a diamond [11].

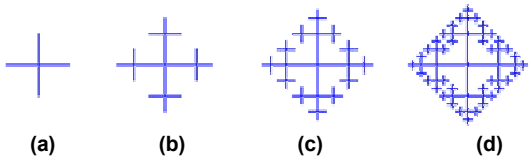

Fig. (1) First three iterations of the construction of the plusses fractal geometry (a) Iteration 0, (b) Iteration 1, (c) Iteration 2 and (d) Iteration 3

3. Design and Simulation of the Proposed Antenna

A plusses patch antenna with two Pairs of orthogonal feeds at x=2.0mm and y=2.0mm is shown in Fig. (2b), and using substrate FR4 with a relative dielectric constant, ε_r=4.4, a substrate height, h=1.6mm, loss tangent, tanδ=0.019, and the dimensions of the dielectric layer are 34x34mm^2. The width of the antenna trace (w) has been chosen to be 2mm. In this work, microwave office (MOW 2007 v7.5) is used to perform a detailed study of voltage standing wave ratio (VSWR), return loss (S_{11}), and radiation field pattern of the proposed Plusses fractal antenna. Figure (2) shows the two and three dimension of the first iteration plusses fractal patch microstrip antenna.

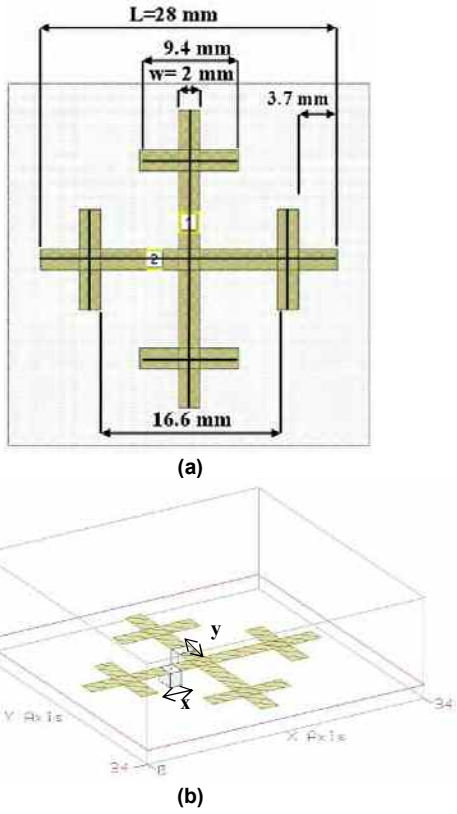

Fig. (2) The proposed antenna (a) Two dimensional view of proposed antenna and (b) Three dimensional view of proposed antenna

At first, a plusses antenna has been modeled with a side length, L of 24mm. Depicted in Fig. (3), the return loss, S_{11} response of this model shows an obvious multiband behavior with first resonance frequency at 2.95GHz.

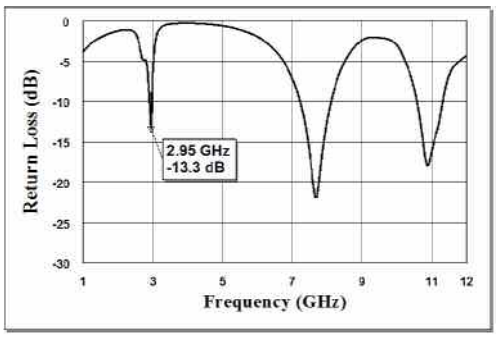

Fig. (3) Simulated return loss of the proposed antenna with side length, L of 24mm

Using the concept of dimension scaling [5], this initial structure is then frequency scaled to the desired frequency, 2.45GHz. The resulting plusses antenna has been found to have a side length of 28mm. The corresponding return loss and VSWR responses of this antenna are depicted in Figs. (4) and (5), respectively.

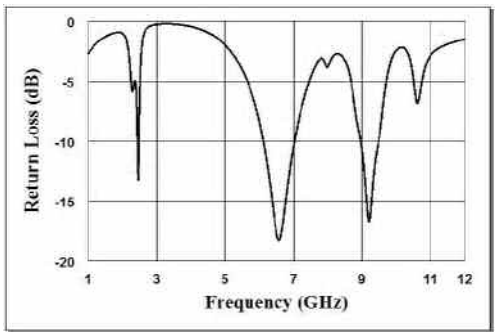

Fig. (4) Simulated return loss of the proposed antenna with side length, L of 28mm

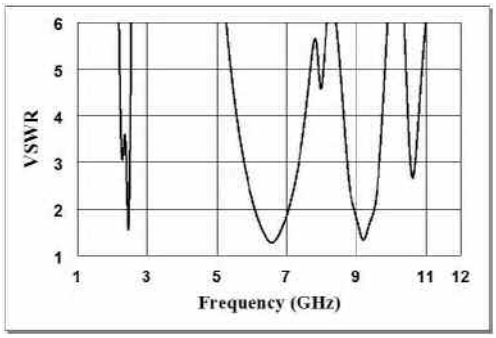

Fig. (5) Simulated VSWR of the proposed antenna with side length, L of 28mm

The first resonance takes place at a frequency of approximately 2.45GHz, where the multi-resonant behavior is very clear. There are three different resonant frequencies, for $S_{11}\leq$-10dB (VSWR$\leq$2) with reasonable bandwidths around each. These frequencies are 2.46, 6.58 and 9.2GHz, respectively, throughout a swept frequency range from 1 to 12GHz.

Figure (6) shows an enlarged copy of Fig. (4). The result of the return loss of a plusses patch antenna design has a good result at frequency of 2.46GHz which is -13.3dB which could be considered as a good result. Where at the resonant frequency of 2.45GHz which is the intended desired frequency has a value of -12.8dB. This result could be considered as fine results. Table (1) shows these resonant frequencies, VSWR, and return loss (S_{11}) with bandwidth of each one.

Table (1) Simulation results for proposed antenna

Resonant frequencies (GHz)		RL (dB)	VSWR	BW (%)
f_{01}	2.46	-13.3	1.55	1.71
f_{02}	6.58	-18.3	1.28	13.8
f_{03}	9.2	-16.7	1.34	5.66

The radiation patterns at these resonant frequencies in copolar and cross-polar components in the E-plane and H-plane are depicted in Fig. (7).

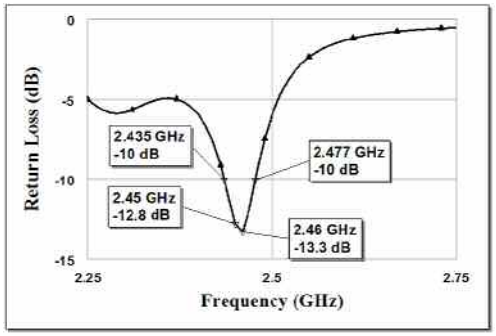

Fig. (6) An enlarged copy of Fig. (4). Simulated return loss at the first resonant, 2.46GHz of the plusses antenna

4. Conclusion

A novel Plusses fractal patch microstrip antenna for multiband wireless communications systems has been designed. The proposed antenna structure showed high degree of self-similarity and space-filling properties. The proposed antenna has triple resonance bands at frequencies of 2.46GHz, 6.58GHz and 9.2GHz, and at these frequencies the antenna has $S_{11}\leq$-10dB (VSWR$\leq$2). According to these frequencies this antenna can operate as a multiband antenna in the microwave frequencies applications.

References

[1] B.B. Mandelbort, "**The Fractal Geometry of Nature**", W.H. Freeman, (1983).

[2] D.L. Jaggard, "**On Fractal Electrodynamics**", in H.N. Kritikos and D.L. Jaggard (eds.), Recent Advances in Electromagnetic Theory, Springer-Verlag, (1990), 183-224.

[3] D.L. Jaggard, "**Fractal Electrodynamics: From Super Antennas to Super lattices**", in J.L. Vehel, E. Lutton, and C. Tricot (eds.), Fractals in Engineering, Springer-Verlag, (1990), 204-221.

[4] J.P. Gianvittorio, "Fractals, MEMS, and FSS Electromagnetic Devices: Miniaturization and Multiple Resonances," Ph.D. Thesis, University of California (2003).

[5] G. Kumar, "**Broadband Microstrip Antennas**," Artech House, Inc. (2003) 63-65.

[6] A.K. Shrivervik, J.F. Zurcher, O. Staub and J.R. Mosig, "PCS Antenna Design: The Challenge of Miniaturization," IEEE Antennas and Propagation Magazine, Vol. 43, (2001) 12-27.

[7] G. Kosiavas et al., "The C-Patch: A Small Microstrip Antenna Element", Electron. Lett., Vol. 25 (1989) 253-254.

[8] V. Palaniswamy and R. Crag, "Rectangular Ring and H-Shape Microstrip Antenna; Alternative Approach to Rectangular Microstrip Antenna", Electron. Lett., Vol. 21 (1985) 874-876.

[9] W.S. Chen, "A Novel Broadband Design of a Printed Rectangular Slot Antenna for Wireless Applications", Microwave Journal, January 2006, Reprinted by Horizon House Publications, Inc. (2006).

[10] S.E. El-Khamy, "New Trends in Wireless Multimedia Communications Based on Chaos and Fractals", 21st National Radio Science Conference (NRSC2004), INV1 1-25, 16-18 March (2004).

[11] http://www.tierrasimbolica.com/apeiron-jun2001/fractals.htm

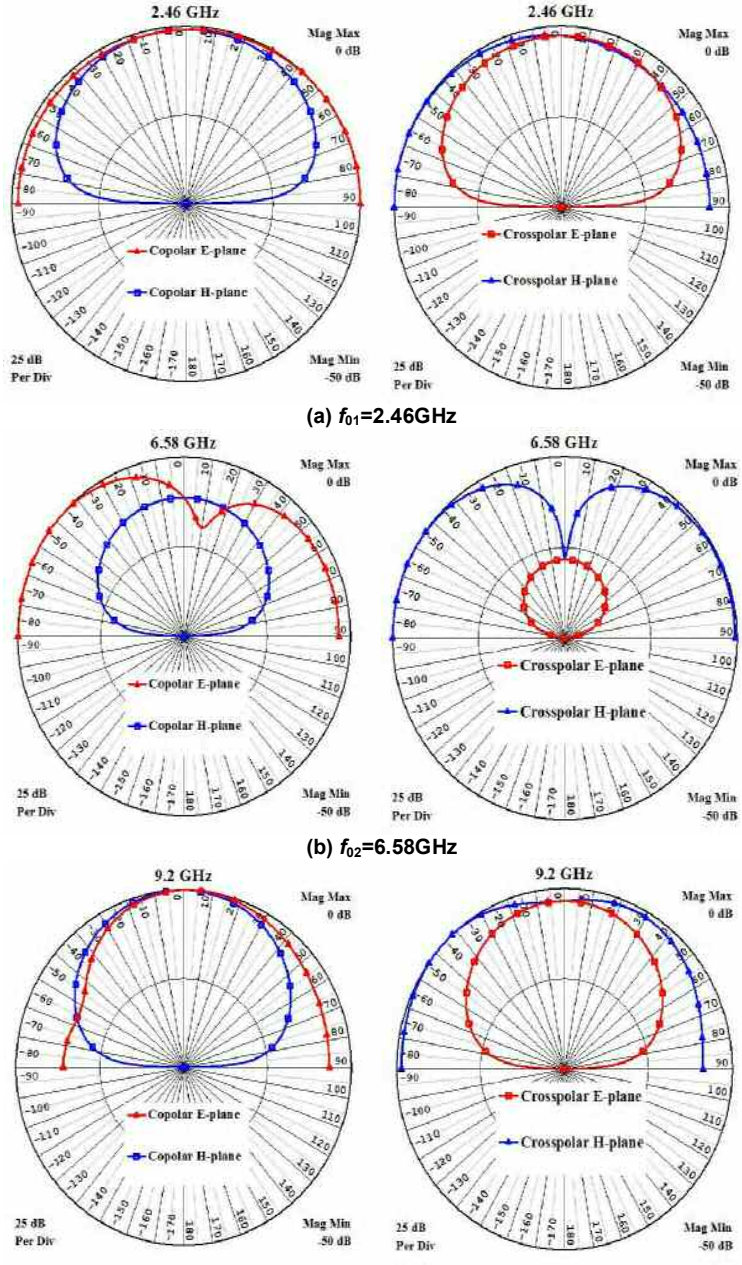

(a) f_{01}=2.46GHz

(b) f_{02}=6.58GHz

(c) f_{03}=9.2GHz

Fig. (7) Radiation patterns of the modeled antenna at resonant frequencies of (a) 2.46GHz (b) 6.58GHz (c) 9.2GHz

Invited Contribution

New Glasses for Optical Fibres and Their Applications

Donald N. Payne

Optoelectronics Research Centre, University of Southampton, Southampton, UK

Keywords: *Optical fibers, Glassess, Refractive index*
Received: 26 September 2009

1. Introduction

Over the past three decades, optical fibres based on high-purity silica have established themselves as perhaps the ultimate communications material. These global cobwebs of glass have revolutionized telecommunications, reaching virtually every populated region on earth and providing enormous bandwidth, the full extend of which has yet to be exploited. Passive waveguides are today being spliced together with lengths of fibre doped with the rare-earth ion erbium, providing optical fibre amplifiers which can boost a fading signal by three orders of magnitude. This combination of active and passive waveguides has made possible all-optical networks, with no electrical/optical interfaces except at the signal source and receiver and paved the way for global optical fibre telecommunications.

Although silica has proved to be ideal for low-loss fibres, it is rarely optimal for functional devices in either fibre or planar waveguide configuration. Silica has particularly low acousto-optic merit, small optical nonlinearity and tiny electro- and magneto- optical coefficients. As a rare-earth host for amplifiers and lasers, it has exceptionally high phonon energy, which leads to non-radiative decay of the excited states, giving rise to poor pump efficiency and in many cases rendering a particular transition unusable. The latter is illustrated by the praseodymium-doped 1.3μm fibre amplifier where a low phonon-energy host, (such as ZBLAN) must be used.

A virtually infinite range of compound glasses is available from which to tailor the properties to suit a particular application. This paper gives examples of research into germanate, telluride, sulphide, mixed-halide and chalcohalide glasses which have been developed as substitutes for silica fibres in specific applications. In particular, it concentrates on research for glasses to use in a practical 1.3μm optical fibre amplifier, as a host for erbium in a planar lossiess splitter, as highly nonlinear materials and in acoustically-efficient devices.

2. Low Phonon-Energy Glasses

It transpires that most of the requirements for optimised fibre and planar devices 1 can be met by glasses having a phonon-energy below about 300cm^{-1} (cf. silica with ~1000cm^{-1} and ZBLAN 600cm^{-1}). When doped with rare-earths, such glasses exhibit efficient radiative transitions at wavelengths as long as 4μm (corresponding to closely-spaced energy levels) without serious competition from phonon-mediated de-excitation. Since the transmission of the glass in the infra-red is also usually limited by the multi-phonon absorption edge, low phonon-energy glasses also have excellent infra-red transmission and can thus form the basis of lasers in the commercially-important 3-5μm wavelength region where the applications are for monitoring of gaseous pollutants.

Low phonon-energy glasses are also invariably composed of compounds having a high reduced-mass, e.g. heavy metals, chlorides and sulphides. As a consequence, they have refractive indices in excess of 2.2, which leads to an optical non-linearity up to two orders of magnitude greater than silica. In addition, the acousto-optic merit can be 1000x that of silica, making them attractive for acousto-optic waveguide switches.

It has been shown that praseodymium-doped ZBLAN glass fibre has potential for a 1.3μm

ISSN 1999-656X PRINTED IN IRAQ

fibre amplifier. However, even in this glass which has a relatively low phonon energy compared to that of silica, 96% of the pump power is lost as heat in the glass to the competing process of multi-phonon decay. The correspondingly-high pump power has hampered the emergence of a suitable commercial device. A world-wide effort is therefore aimed at developing a lower phonon-energy glass to increase the pump efficiency to perhaps 1dB/μW (cf. EDFA as high as 11dB/mW). The search for a suitable host has targeted glasses such as the halides and sulphides, all of which offer good transmission in the infra-red, reasonable transparency at the pump wavelength (around 1μm) and good chemical durability. Extensive work based on fluoride glasses modified with indium and gallium show only a 2 slight improvement over the fluorozirconate glasses, while substitution of the heavier chlorine for fluorine (as in the mixed cadmium halide glasses) show efficiencies up to 10%. Unfortunately, these materials are unstable and are rapidly attacked by moisture.

Work has concentrated on the gallium lanthanum sulphide glasses in which quantum efficiencies as high as 60% are indicated. Progress is such that glass batches approaching a kg can now be melted and multi-mode fibres of several hundred metres drawn. Fibre drawing is particularly challenging as these glasses have a very high viscosity at temperatures below the onset of crystallisation.

3. Low Index Glasses

A second candidate for an efficient 1.3μm is Nd-doped low-index glass. Up to now the 1.3μm transition in neodymium has been discarded as having a gain peak at too long a wavelength (1400nm in silica, 1340nm in ZBLAN). Generally, more ionic glasses tend to shift the emission spectrum of neodymium towards shorter wavelengths and these glasses are characterised by having a low index. The glass with lowest known index is a fluoro-beryllate composition, which has the disadvantage of being highly toxic, environmentally unstable and difficult to draw. Recently, however we have found that glasses in the alumino-fluorophosphate system which have gain peaks in the region of 1317nm, which coincides almost exactly with the wavelength of zero dispersion in most installed fibres. These glasses are chemically durable, stable against crystallisation and straightforward to draw.

Nd-doped glasses have a number of advantages for 1.3μm amplifiers. High concentrations (several percent) can be incorporated without fear of upconversion effects, leading to amplifiers of only a centimetre or so long. As well as obviating the need for a low-loss fibre, planar amplifier devices are readily achievable. We hare drawn fibres with losses less than l dB/m and demonstrated gain of several dB in single-mode fibres. The challenge now is to reduce the competing amplified spontaneous-emission from the more-favoured 1.06μm transition by continuous filtering along the length of the amplifier. Computations based on numerous spectroscopic measurements indicate that a pump efficiency of l dB/mW is within reach.

4. Other Glasses

As well as the above examples of the importance of new glasses for guided-wave devices, work on other interesting glass compositions will be reviewed. These include so-called "spaghetti glasses', heavy-metal oxide glasses and chalcohalides. While none of these glasses are expected to compete with silica as a low-loss transmission medium, they have unique properties at longer wavelengths and are expected to find applications in devices where relatively-short lengths are used.

5. Conclusions

Glasses with high-refractive index, high acousto-optic merit, low phonon energy and good solubility of the rare-earth are essential for optical waveguides devices of the future. At the ORC, research on advanced materials for multi-function waveguides is driven by device requirements. A more efficient optical fibre amplifier for 1.3μm requires new glasses of lower vibrational energies to minimise nonradiative decay. Planar lossless splitters rely on a new waveguide material which allows high incorporation of erbium. Modulators need bulk or fibre optics which interact with acousto-optic power. Other new glasses with very high photosensitivity are being developed for fibre Bragg gratings, and highly non-linear glasses for all-optical switches. It is clear that for functions as diverse as amplification, splitting, modulation, switching or filtering the key to these devices is new glass materials.

Structural and Optical Characteristics of CdSe Thin Films Prepared by Chemical Bath Deposition Technique

K. Girija [1]
S. Thirumalairajan [1]
S.M. Mohan [2]
J. Chandrasekaran [2]

[1] *Department of Nanoscience and Technology, School of Physical Science, Bharathiar University, Coimbatore, Tamil Nadu, India*
[2] *Department of Physics, Sri Ramakrishna Mission Vidyalaya College of Arts and Science, Coimbatore, Tamil Nadu, India*

Cadmium selenide thin films were deposited on glass substrate using chemical bath technique for different bath temperatures 313K, 333K and 353K. Polycrystalline nature of the material was confirmed by X-ray diffraction technique and various structural parameters were calculated. The optical properties were revealed by UV-Visible transmittance spectra and the band gap energy was determined.

Keywords*: Thin films, CdSe, X-ray diffraction, Scanning electron microscopy, Optical properties*
Received: 2 September 2009, **Revised**: 28 September 2009, **Accepted**: 5 October 2009

1. Introduction

The II-VI binary semiconducting compounds belonging to the cadmium chalcogenide family (CdS, CdSe, CdTe) are considered to be very important materials for photovoltaic applications [1-3]. CdSe is a promising photovoltaic material because of its high absorption coefficient and nearly optimum band gap energy for the efficient absorption of light and conversion into electrical power [4]. CdSe has been extensively investigated for its potential applications in photoelectrochemical (PEC) solar cell, optoelectronic devices and gamma ray detectors [5-7]. CdSe is an important material for the development of various modern technologies of solid state devices such as high efficiency thin film transistors and light emitting diodes. Other areas of successful applications include photo-detectors, light amplifiers, lasers, gas sensors, large-screen liquid crystal display and photoluminescence response [8]. Semiconductor devices based on CdSe thin films strongly depend on the structural and optical properties of the films obtained from various experimental conditions. A direct band gap range of 1.65 eV-1.84 eV has been reported for CdSe by various authors [9-10] and its photosensitivity gives it an edge over other semiconducting materials. Several physical and chemical techniques are available for the growth of CdSe thin films. CdSe thin films have been deposited using different techniques such as electrodeposition [11-12], molecular beam epitaxy [13], spray pyrolysis [14], successive ionic layer adsorption and reaction method [15], vacuum deposition and chemical bath deposition [16]. Among these methods chemical bath deposition has several overriding advantages with other techniques such as uniform film deposition, control of thickness, precise maintenance of deposition temperature, low cost [17-18]. The deposition parameters are usually optimized to obtain specularly reflecting films with a good adherence to the substrate [19-21].

In the present investigation, chemical bath deposition of cadmium selenide thin films has been reported. Structural characterization from XRD, EDAX and optical characterization from UV-Vis were carried out.

2. Experiment

Chemical bath deposition technique was adopted for the preparation of cadmium selenide (CdSe) thin films. The chemicals used for the preparation were analytical grade cadmium

acetate (99%), selenium powder (99.5%) and sodium sulphite (98%).

The reaction mixture was prepared by adding ammonia (NH_3) solution in 0.1 M of cadmium acetate [$(CH_3COO)_2Cd.2H_2O$] till a pH of 11 is attained. To the precursor cadmium acetate-ammonia solution, 5ml of freshly prepared sodiumselenosulphite (Na_2SeSO_3) diluted with 5ml of distilled water was added drop by drop under continuous gentle stirring using magnetic stirrer at about 80±1rpm. Sodium selenosulphite was prepared by refluxing 4gm of selenium powder with 12gm of anhydrous sodium sulphite (Na_2SO_3) in 50ml of double distilled demineralised water for 4 hours at 80±0.5°C. Thoroughly cleaned glass substrates were vertically immersed at the centre of the reaction bath.

The deposition of the film was carried out at bath temperatures 313K, 333K and 353K. The bath temperature was controlled using a digital thermostat connected with Pt-100 thermocouple. The colourless bath turned orange in colour and then to orange-red as time progressed. The time of deposition was optimized as 130min. After deposition, the substrates were rinsed in distilled water and dried. The films were then annealed in air at a temperature of 553K for 15min. During annealing the colour of the film changed from orange to red then to dark brown. Films prepared by this method were uniform, well adherent to the substrate, smooth and reflecting.

At intermediate temperature (333K), the ions get sufficient time to condense on the substrate surface and therefore large amount of material gets deposited on the substrate giving maximum layer thickness. At relatively higher temperatures, more and more ions are released but all the ions do not get chance to adsorb on the substrate surface, they settle down at the bottom of the reaction container decreasing the film thickness [22].

The CdSe films were structurally characterized by X-ray powder diffraction using a JEOL JDX services instrument with CuK_α radiation (λ=1.5406Å). The microstructures of these samples were characterized using Hitachi S-3400 equipped with an EDAX spectrometer. The optical properties of CdSe films were measured using UV-Vis spectrophotometer (JASCO V-530 dual beam).

3. Results and discussion

The structural elucidation of CdSe film for the bath temperatures 333K and 353K are presented in Fig. (1) with the diffraction 2θ from 20 to 70°C. The observed *d* spacing and the respective prominent peaks correspond to reflections from (111), (220) and (311) planes which coincide well with JCPDS data [23]. Therefore it has been concluded that the deposited CdSe thin films are polycrystalline in nature with cubic structure. The lattice parameter (a) for cubic structure is determined using the relation

$$a = d\sqrt{h^2 + k^2 + l^2} \quad (1)$$

where, d is the spacing between the planes in the atomic lattice, *hkl* are the Miller indices

The grain size (D) for CdSe thin films are calculated using Scherrer's formula

$$D = \frac{k\lambda}{\beta \cos\theta} \quad (2)$$

where, the constant k is the shape factor, taken as 0.94, λ is the wavelength of X-rays (1.5406Å for CuK_α), θ is the Bragg's angle and β is the full width at half maximum

The dislocation density (δ) has been evaluated from Williamson and Smallman's formula $\delta=1/D^2$ (lines/m^2). The micro strain (ε) is obtained using the relation $\varepsilon=\beta\cos\theta/4$.

All these parameters are calculated and presented in Table (1).

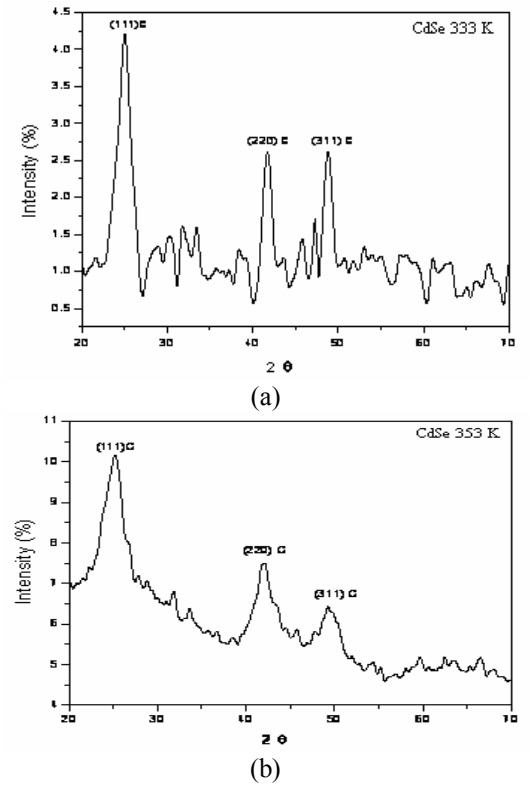

Fig. (1) (a) XRD pattern of CdSe thin film (333K), (b) XRD pattern of CdSe thin film (353K)

Table (1) Structural Parameters of CdSe Thin Film

Material (temp. in K)	2θ (deg)	d (spacing) Å	(β) FWHM	(*hkl*)	Lattice (a) Å	Grain Size(D) nm	density (δ) $x10^{15}$ lines/m^2	Micro strain (ε) $x10^{-3}$
	25.3436	3.51438	1.170	111	6.0870	7.2701	18.9193	4.9798
CdSe (333K)	42.1084	2.11360	1.160	220	5.9781	7.6660	17.0160	4.7226
	49.8257	1.8286	1.152	311	6.0647	7.9430	15.8499	4.5579
	25.2062	3.53030	1.152	111	6.1146	7.3818	18.3516	4.9045
CdSe (353K)	42.0122	2.14887	1.152	220	6.0779	7.7167	16.7930	4.6916
	49.6925	1.8046	1.142	311	5.9851	8.0082	15.5927	4.5208

The quantitative analysis of CdSe films prepared at bath temperature 333K is shown in Fig. (2). The EDAX pattern confirms the presence of cadmium and selenide compounds. The average atomic percentage ratio of CdSe was found to be 19.57:3.78 showing that the sample was cadmium rich. Presence of silicon in EDAX is due to the silicon content in glass substrate, since Na_2SeSO_3 was used as a source of selenium, a small amount of sodium is present in the film where as sulphur escapes as H_2S or SO_2.

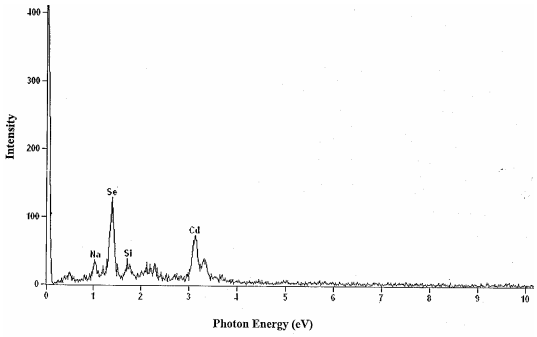

Fig. (2) Energy Dispersive X-ray analysis of CdSe thin film (333 K)

The optical transmittance spectra of CdSe thin film is recorded as a function of wavelength in the range 400-1200 nm as shown in Fig. (3). The CdSe material deposited on the glass substrate showed a transmittance of ~60 % for 313 K and is found to decrease as temperature increases along with the film thickness which shows the improvement in crystallinity. A typical plot of $(\alpha h\nu)^2$ with photon energy hν for CdSe thin film is shown in Fig. (4). The band gap energy is obtained by extrapolating the straight line portion of the graph to zero absorption coefficient. The intercept on the *hν* axis gives the value of band gap energy. It was found to be 2.12eV, 1.75eV and 1.52eV at bath temperatures 313K, 333K and 353K respectively. The direct band gap energy was found to decrease as temperature increases along with film thickness [16]. These changes are attributed to the crystallite size - dependent properties of the band gap energy.

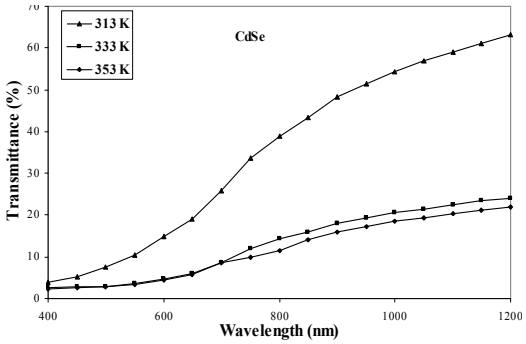

Fig. (3) Transmittance of CdSe

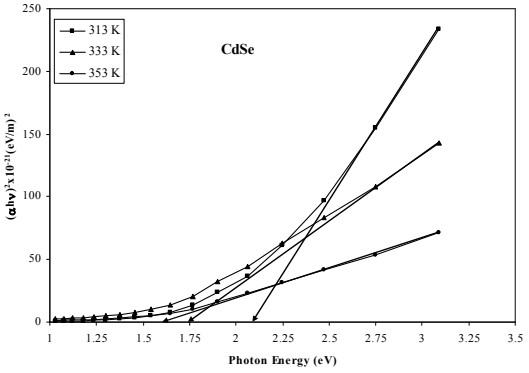

Fig. (4) Band gap energy of CdSe

4. Conclusions

CdSe thin films were deposited onto glass substrate by simple economical chemical bath deposition technique at bath temperatures 313K, 333K and 353K. XRD pattern confirms the cubic structure of CdSe thin film. SEM analysis revealed the presence of spherical shaped clusters of size 1.11μm. The presence of Cd and Se elements were confirmed from EDAX analysis. From the optical analysis the band gap energy was found to lie in the range 2.12eV - 1.52eV.

References

[1] X. Mathew et al., *Solar Energy*, 77 (2004) 831.
[2] E. Benamar et al., *Ann. Chim. Sci. Mater.*, 23 (1998) 369.
[3] D.J. Peno et al., *J. Phys. Chem.*, B 106 (2002) 7458.

[4] V. Antonucci et al., *Solar Cells*, 31 (1999) 119.
[5] Y.A. Afuzov, E.T. Bilyalov, V.M. Sviriuv, *Galiotekhinika*, 4 (1984) 69.
[6] S. Uthana and P.J. Reddy, *phys. status solidi*. A65 (1981) 269.
[7] A.K. Rautri et al., *Thin Solid Films*, 91 (1982) 55.
[8] P.P. Hankare et al., *J. Phys. Chem. Solid*, 67 (2006) 2506.
[9] C. Baban, G.I. Rusu and P. Prepelita, *J. Optoelectron. Adv. Mater.*, 7 (2005) 817.
[10] R. Blargava, **"Properties of Wide Band Gap II-VI Semiconductors"**, INSPEC Publications, London, U.K. (1997).
[11] K.R. Murali et al., *J. Electroanal. Chem.*, 95 (1995) 368.
[12] K.R. Murali et al., *J. Electroanal. Chem.*, 261 (1991) 303.
[13] N. Samarth et al., *Appl. Phys. Lett.*, 2680 (1989) 54.
[14] T. Elango, S. Subramanian and K.R. Murali, *Surf. Coat. Technol.*, 8 (2003) 123.
[15] C.D. Lokhande et al., *Appl. Surf. Sci.*, 413 (2001) 182.
[16] S. Erat, H. Metin and M. Ari, *Mater. Chem. and Phys.*, 111 (2008) 114.
[17] A.M. Salem, *Appl. Phys.*, A 74, 205 (2002).
[18] J. McAleese and P. O'Brien, *J. Mater. Chem.*, 8 (1998) 2309.
[19] G. Hodes et al., *Phys. Rev.*, B 36 (1987) 4215.
[20] F. Trojanek et al., *J. Crystal Growth*, 209 (2000) 695.
[21] P. Nemec et al., *J. Crystal Growth*, 240 (2002) 484.
[22] R.C. Kainthila, D.K. Pandya and K.L. Chopra, *J. of Electrochem. Soc.*, 277 (1980).
[23] JCPDS File No: 19 - 0191 and 08 - 459.

A Boubaker Polynomials Expansion Scheme BPES-Related Analytical Solution to Williams-Brinkmann Stagnation Point Flow Equation at a Blunt Body

D.H. Zhang [1]
F.W. Li

[1] *Department of Physics, South China University, Guangzhou, 510642 China*

An analytic solution is proposed for the problem of Williams-Brinkmann axisymmetric steady flow in vicinity of a stagnation point at a blunt body. The boundary equations governing the flow are embedded in the main equation system by the mean of the Boubaker Polynomials Expansion Scheme (BPES). The main differential equations are solved analytically and yield continue and differentiable C_∞ solutions which are compared to some published ones so far.

Keywords: *Polynomial expansion, Stagnation point, Flow equation, BPES*
Received: 22 October 2009, **Revised**: 29 October 2009, **Accepted**: 1 November 2009

1. Introduction

Williams-Brinkmann stagnation point flow problem is related to a flow which encounters an obstacle or is stagnated by a wall. The equations that govern this problem are encountered in several studies in applied physics fields [1-0]. The majority of the proposed solution is numerical or based on numerical analyses. In this context, several interesting investigations can be cited, as the works of Nasr *et al.* [1], Orszag [2] focused on spectral methods for yielding numerical solutions, the studies of White [3], Wadia *et al.* [4], Rosenhead [5] and Beckett [6] which exploited the finite difference methods, and the results concerning the 2D stagnation point flow problem published by Mahapatra *et al.* [7,8], Wang [9] and Lok *et al.* [10].

In the two last decades' related literature, some less numerous attempts to propose analytical or so-called exact solution have been performed [11-16]. In the present work, an analytical continuous solution, based on the Boubaker Polynomials Expansion scheme (BPES) [17-37], is proposed. The analysis is presented with reference to the nonlinear coupled differential equations governing the flow of an incompressible viscous fluid in the vicinity of the forward stagnation point at a blunt body. Results for the given relevant parameters are plotted and are found to be in good agreement with some results available in the last decades' literature [2-16].

2. Basic equations system

The general system of differential equations governing the motion of an incompressible viscous fluid near a stagnation point at a blunt body can be obtained by considering a two-dimensional flow of an incompressible fluid of kinematic viscosity $\vec{\varpi}$ which impinges vertically (Fig. 1) toward the plane z=0.

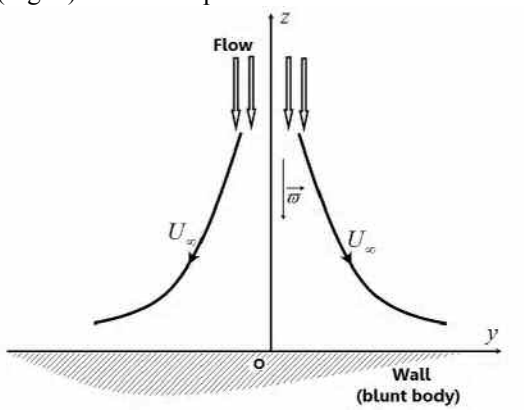

Fig. (1) Stagnation point scheme

Due to the local uniform vertical velocity $\varpi = -A \times z$, where A is the constant velocity gradient in the outer flow far away from the plate, the flow symmetrically divides into two streams along positive and negative y axis on the wall, creating a stagnation point at O(y=0;z=0). The Williams-Brinkmann equations [2-15] are hence:

$$\begin{cases} f''' + (f+Cg)f'' - f'^2 = -1 \\ Cg''' + C(f+Cg)g'' + C^2 = 0 \\ f'' + Cg'' + (ff' + Cf'g + Cfg' + C^2 gg') = \frac{1}{2}(1+2C+C^2)F' \end{cases} \quad (1)$$

where f' and g' are the dimensionless velocity components in the x and z directions, F is the dimensionless pressure function and C is a constant.

Under the assumptions of Wu *et al.* [38] and Kumaran *et al.* [39], for an axisymmetric steady motion (C=1 and f=g), and by setting:

$$\begin{cases} f = f(\varepsilon) = \dfrac{\psi(y,z)}{y\sqrt{A\varpi}} \\ \varepsilon = z\sqrt{\dfrac{A}{\varpi}} \end{cases} \quad (2)$$

where $\psi(y,z)$ is the stream function, it gives the simplified system:

$$\begin{cases} f'''(\varepsilon) + 2f(\varepsilon)f''(\varepsilon) - \left(f'(\varepsilon)\right)^2 = -1 \\ f''(\varepsilon) + 2f(\varepsilon)f'(\varepsilon) = 2F'(\varepsilon)' \\ \varepsilon \in [0;\varepsilon_{\max}] \end{cases} \quad (3)$$

with simplified boundary condition:

$$\begin{cases} f(\varepsilon)\big|_{\varepsilon=0} = 0 \\ F(\varepsilon)\big|_{\varepsilon=0} = 0 \\ \lim\limits_{\varepsilon\to+\infty} \dfrac{df}{d\varepsilon}(\varepsilon) \approx \dfrac{df}{d\varepsilon}(\varepsilon)\Big|_{\varepsilon=\varepsilon_{\max}} = 1 \end{cases} \quad (4)$$

3. Solution Derivation Using the BPES

With respect to the earliest definition of the 4q-Boubaker polynomials expansion scheme (BPES) [17-37], for a complex function $f(\varepsilon)$ of a real argument ε, the resolution protocol is carried out by applying the expressions:

$$\begin{cases} f(\varepsilon) = \dfrac{1}{2N_0}\sum\limits_{q=1}^{N_0} \xi_q \times B_{4q}(\hat{\varepsilon}_q) \\ F(\varepsilon) = \dfrac{1}{2N_0}\sum\limits_{q=1}^{N_0} \xi_q' \times B_{4q}(\hat{\varepsilon}_q) \\ \hat{\varepsilon}_q = -\dfrac{\alpha_q}{\varepsilon_{\max}}\left(\varepsilon - \varepsilon_{\max}\right); \hat{\varepsilon}_q \in [0;\alpha_q] \end{cases} \quad (5)$$

where α_q is 4q-Boubaker polynomial minimal root, N_0 is a prefixed integer, ξ_q and ξ_q' (q=1, ..., N_0) are unknown coefficients.

The BPES formulation has the advantage of embedding the boundary conditions (4) intrinsically and prior to resolution process:

$$\begin{cases} f(\varepsilon)\big|_{\varepsilon=0} = \dfrac{1}{N_0}\sum\limits_{q=1}^{N_0} \xi_q B_{4q}(\alpha_q) = 0; \\ F(\varepsilon)\big|_{\varepsilon=0} F(\varepsilon) = \dfrac{1}{2N_0}\sum\limits_{q=1}^{N_0} \xi_q' \times B_{4q}(\alpha_q) = 0; \\ f'(\varepsilon)\big|_{\varepsilon=\varepsilon_{\max}} = \dfrac{1}{2N_0}\sum\limits_{q=1}^{N_0} \xi_q \times (-2) = \dfrac{-1}{N_0}\sum\limits_{q=1}^{N_0} \xi_q = 1 \end{cases} \quad (6)$$

Consequently, the two first boundary conditions (4) are intrinsically verified, while the remaining one induces the additional relation:

$$\sum_{q=1}^{N_0} \xi_q = -N_0 \quad (7)$$

The main equation (3) is then altered to:

$$\sum_{q=1}^{N_0}\left(-\frac{\alpha_q}{\varepsilon_{\max}}\right)^3 \xi_q \frac{d^3 B_{4q}(\hat{\varepsilon}_q)}{d\varepsilon^3} + \frac{1}{N_0}\left(\sum_{q=1}^{N_0} \xi_q B_{4q}(\hat{\varepsilon}_q)\right)\left(\sum_{q=1}^{N_0} \xi_q \left(\frac{\alpha_q}{\varepsilon_{\max}}\right)^2 \frac{d^2 B_{4q}(\hat{\varepsilon}_q)}{d\varepsilon^2}\right) - \left(\sum_{q=1}^{N_0} \xi_q \frac{\alpha_q}{\varepsilon_{\max}} \frac{dB_{4q}(\hat{\varepsilon}_q)}{d\varepsilon}\right)^2 = -2N_0 \quad (8)$$

By integrating the $\hat{\varepsilon}_q$-dependent terms in the interval [0;$\varepsilon_{\max}$], a weak solution is proposed as a solution to the final system:

$$\begin{cases} \min\left\langle [\xi]^T \times [A] \times [\xi] \right\rangle\Big|_{\sum\limits_{q=1}^{N_0} \xi_q = -N_0} \\ [\xi] = \begin{pmatrix} \xi_1 \\ \xi_2 \\ .. \\ \xi_{N_0} \end{pmatrix}, [A] = \begin{pmatrix} a_{11} & a_{12} & .. & a_{1N_0} \\ a_{21} & .. & .. & .. \\ .. & .. & .. & .. \\ a_{N_0 1} & .. & .. & a_{N_0 N_0} \end{pmatrix} \end{cases} \quad (9)$$

where:

$$\begin{cases} a_{ij}\big|_{i\neq j} = \dfrac{1}{N_0}\displaystyle\int_0^{\varepsilon_{\max}} (-\frac{\alpha_j}{\varepsilon_{\max}})^2 B_{4i}(\hat{\varepsilon}_i) \times \frac{d^2 B_{4j}(\hat{\varepsilon}_j)}{d\varepsilon^2} d\varepsilon \\ a_{ij}\big|_{i=j} = -\displaystyle\int_0^{\varepsilon_{\max}} (-\frac{\alpha_i}{\varepsilon_{\max}})^2 \times (\frac{dB_{4i}(\hat{\varepsilon}_i)}{d\varepsilon})^2 d\varepsilon \end{cases} \quad (10)$$

The solution is hence the proper vector $[\xi]_{\lambda\min}$ which corresponds to the minimal proper value $\lambda_{\min}$ of the matrix $[A]$, subjected to the normative condition: $\sum\limits_{q=1}^{N_0} \xi_q = -N_0$:

$$\begin{cases} f(\varepsilon) = \dfrac{1}{2N_0}\displaystyle\sum_{q=1}^{N_0} \xi_{q,\lambda_{\min}} \times B_{4q}(\hat{\varepsilon}_q) \\ \hat{\varepsilon}_q = -\dfrac{\alpha_q}{\varepsilon_{\max}}(\varepsilon - \varepsilon_{\max}); \hat{\varepsilon}_q \in [0;\alpha_q] \end{cases} \quad (11)$$

The coefficients ξ_q' (q=1, ..., N_0), which give the value of , are obtained by identification, as solutions to the equation:

$$\sum_{q=1}^{N_0} \xi_q' \times \frac{dB_{4q}(\hat{\varepsilon}_q)}{d\varepsilon} = \frac{1}{2}\sum_{q=1}^{N_0} \xi_{\xi_{q,\lambda_{\min}}} \left(\frac{\alpha_q}{\varepsilon_{\max}}\right)^2 \frac{d^2 B_{4q}(\hat{\varepsilon}_q)}{d\varepsilon^2} + \frac{1}{2N_0}\left(\sum_{q=1}^{N_0} \xi_{\xi_{q,\lambda_{\min}}} \frac{\alpha_q}{\varepsilon_{\max}} \frac{dB_{4q}(\hat{\varepsilon}_q)}{d\varepsilon}\right)\left(\sum_{q=1}^{N_0} \xi_{\xi_{q,\lambda_{\min}}} B_{4q}(\hat{\varepsilon}_q)\right)$$

The solution $f(\varepsilon)$ and $f'(\varepsilon)$ is plotted in Fig. (2), in the case of an axisymmetric steady motion (C=1, ε_{max}=5):

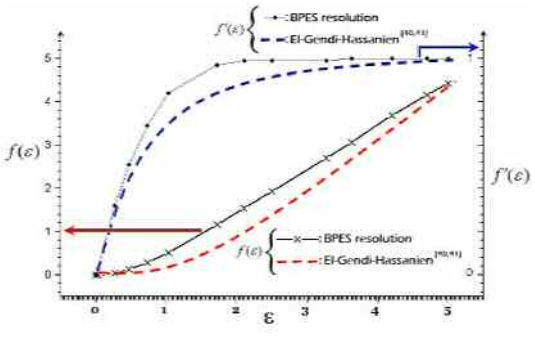

Fig. (2) Solution plots

Variations of the dimensionless pressure function $F(\varepsilon)$ are plotted in Fig. (3).

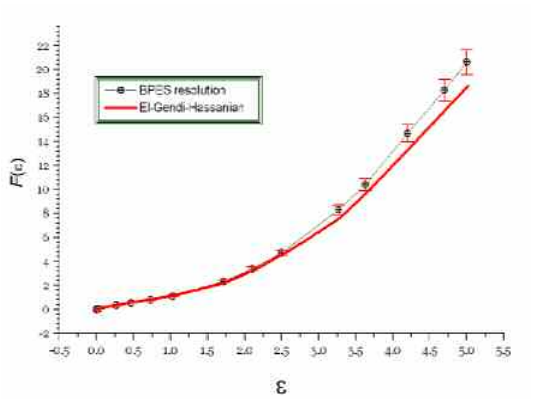

Fig. (3) Dimensionless pressure plots

4. Discussion and comparison

The curves of the proposed solution ($f(\varepsilon)$ and $f'(\varepsilon)$, Fig. 2) are in good agreement with the plots proposed earlier by El-Gendi [40] and Hassanien [41], particularly at edges. This noticed agreement is also verifiable for the dimensionless pressure function $F(\varepsilon)$.

In order to endorse these notes, and for enabling deeper comparison, values of skin frictions $f''(0)(=g''(0))$, as well as $F'(0)$, have been gathered in Table (1) along with results provided by other authors [41-44].

5. Conclusion

In the present work, an expansion procedure based on a polynomial approximation for the solution of Williams-Brinkmann axisymmetric steady flow boundary value problem is introduced. The analysis is presented with reference to the nonlinear coupled differential equations governing the fluid flow in the vicinity of the forward stagnation point at a blunt body. Results for different particular cases are obtained and are found to be in very good agreement with other published ones.

Table (1) Compared initial values

	$f''(0)$	$F'(0)$
BPES Result	1.311938	0.94320
I. A. Hassanien[41]	1.311940	0.94251
H. W. Cheng *et al.*[42]	1.31192	--
H. Schlichting[43]	1.3119	--

Acknowledgement

The authors acknowledge the support and the hints from Prof. K. Boubaker from Department of Physics-ESSTT, Tunisia, and Dr T. Ortega from UPDE-Panama City, Panama.

References

[1] H. Nasr, I.A. Hassanien and H.M. El-Hawary, *Inter. J. Comp. Math.,* 33 (1990) 127.
[2] S.A. Orszag, *J. Comp. Phys.* 37 (1980) 70.
[3] F.M. White, **"Viscous FIuid Flow"**, McGraw-Hill, Inc. (1974).
[4] R. Wadia and F.R. Payne, *Intern. J. Computer Math.*, 9 (1981) 163.
[5] L. Rosenhead, **"Laminar Boundary Layers"**, Oxford University Press (1963).
[6] P.M. Beckett, *Int. J. Computer Math.* 14 (1983) 282.
[7] T. Mahapatra and A.S. Gupta, *Can. J. Chem. Eng.* 81 (2003) 258.
[8] T. Mahapatra and A.S. Gupta, *Heat Mass Transf.* 38 (2002) 517.
[9] Y. Lok and N. Amin, *Int. J. Nonlinear Mech.* 41 (2006) 622.
[10] C. Wang, *Int. J. Nonlinear Mech.* 43 (2008) 377.
[11] J.M. Dorrepaal, *J. Fluid Mech.* 163 (1986) 141.

[12] T. Liu, *Quart. Appl. Math*. 50 (1992) 39.
[13] J.T. Stuart, *J. Aero-Space Sci*. 26 (1959) 124.
[14] K. Tamada, *J. Phys. Soc. Japan* 46 (1979) 310.
[15] R. Tsay and S. Weinbaum, *J. Fluid Mech*. 226 (1991) 125.
[16] L. Meirovitch, **"Analytical Methods in Vibrations"**, MacMillan (NY, 1994) 301.
[17] O.D. Oyodum et al., *Euro. Phys. J. Appl. Phys.* (EPJAP), 46(2) (2009) 21201.
[18] O.B. Awojoyogbe and K. Boubaker, *Curr. App. Phys*. 9 (2009) 278.
[19] J. Ghanouchi, H. Labiadh and K. Boubaker, *Int. J. of Heat and Tech*. 26(1) (2008) 49.
[20] S. Slama et al., *Num. Heat Transf. Part A*, 55 (2009) 401.
[21] S. Slama, M. Bouhafs and K. Boubaker, *Int. J. of Heat and Tech*. 26(2) (2008) 141.
[22] S. Slama et al., *Eur. Phys. J. Appl. Phys*. (EPJAP), 44 (2008) 317.
[23] S. Slama et al., *Proc. COTUME'08*, (2008) 79.
[24] S. Fridjine and M. Amlouk, *Modern Phys. Lett. B*23 (2009) 2179.
[25] S. Fridjine, K. Boubaker and M. Amlouk, *Canad. J. of Phys.* 87 (2009) 653.
[26] S. Fridjine et al., *J. Alloys and Comp*. 479 (2009) 457.
[27] S. Tabatabaei et al., *Heat Mass Transf*. 45 (2009) 1247.
[28] Belhadj, O. Onyango and N. Rozibaeva, *J. Thermophys. Heat Transf*. 23 (2009) 639.
[29] Chaouachi et al., *Eur. Phys. J. Appl. Phys*. (EPJAP), 37 (2007) 105.
[30] H. Labiadh et al., *J. of Diff. Eq. & C. Proc*. 1 (2007) 51.
[31] K. Boubaker, *Trends in Appl. Sci. Res.* 2 (2007) 540.
[32] K.B. Ben Mahmoud, *J. of Thermophys. and Heat Transf*. 23 (2009) 409.
[33] K. Boubaker, *Int. J. of Heat and Tech*. 20 (2008) 31.
[34] T.G. Zhao, Y.X. Wang and K.B. Ben Mahmoud, *Int. J. Math. Comp.* 1 (2008) 13.
[35] T. Ghrib, K. Boubaker and M. Bouhafs, *Mod. Phys. Lett. B*22 (2008) 2907.
[36] K. Boubaker, *Far East J. of App. Math*. 31 (2008) 299.
[37] N. Guezmir et al., *J. All. and Comp*. 481 (2009) 543.
[38] Q. Wu, S. Weinbaum and Y. Andreopoulus, *Chem. Eng. Sci.* 60 (2005) 123.
[39] V. Kumaran, R. Tamizharasi and K. Vajravelu, *Commun. Nonlinear. Sci. Numer. Simulat*. 14 (2009) 2677.
[40] S.E. El-Gendi, *Computer J.* 12 (1969) 282.
[41] A. Hassanien, *Energy Convers. Mgmt*. 38 (1997) 839.
[42] H.W. Cheng, M.N. Ozisik and J.C. Williams III, *ASME J. Appl. Mech.* 38 (1960) 282.
[43] H. Schlichting, **"Boundary Layer Theory"**, McGraw-Hill (NY, 1960).

Fundamental Understanding of the Propagation of Light Using Geometry

Ahmed K. Alsamarrai

Department of Physics, Faculty of Education, University of Baghdad, Baghdad, Iraq

The treatment of light as wave motion allows for a region of approximation in which the wavelength is considered to be negligible compared with the dimensions of the relevant components of the optical system. This region of approximation is called geometrical optics. When the wave character of the light may not be ignored, the field is known as physical optics. Since the wavelength of light is very small compared to ordinary objects, early unrefined observations of the behavior of a light beam passing through apertures or around obstacles in its path could be handled by geometrical optics.

***Keywords**: Optics, Light propagation, Geometrical optics, Optical path length*
Received: 5 October 2009, **Revised**: 31 October 2009, **Accepted**: 7 November 2009

Within the approximation represented by geometrical optics, light is understood to travel out from its source along straight lines or **rays**. The ray is simply the path along which energy is transmitted from one point to another in an optical system. The ray is a useful, although abstract, construct; perhaps the best approximation to a ray of light is a pencil-like laser beam. When a light ray traverses an optical system consisting of several homogeneous media in sequence, the optical path is a sequence of straight-line segments. The laws of geometrical optics that describe the subsequent direction of the rays are succinctly stated as:

Law of Reflection: When a ray of light is reflected at an interface dividing two uniform media, the reflected ray remains within the **plane of incidence**, and the angle of reflection equals the angle of incidence. The plane of incidence includes the incident ray and the normal to the point of incidence.

Law of Refraction (Snell's Law): When a ray of light is refracted at an interface dividing two uniform media, the transmitted ray remains within the plane of incidence and the sine of the angle of refraction is directly proportional to the sine of the angle of incidence.

These laws can be visually seen in the following figure

Huygens' Principle

The Dutch physicist Christian Huygens imagined each point of a propagating disturbance as capable of originating new pulses that contributed to the disturbance an instant later. To show how his model of light propagation implied the laws of geometrical optics, he formulated a principle which says that **each point on the leading surface of a wave disturbance may be regarded as a secondary source of spherical waves, which themselves progress with the speed of light in the medium and whose envelope at later times constitutes the new wavefront**.

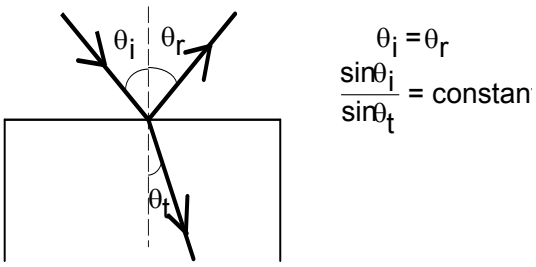

Notice that the new wavefront is tangent to each wavelet at a single point. According to Huygens, the remainder of each wavelet is to be disregarded in the application of the principle. In so disregarding the effectiveness of the overlapping wavelets, Huygens avoided the possibility of diffraction of the light into the region of geometric shadow. Huygens also ignored the wavefront formed by the back half of the wavelets, since these wavefronts implied a light disturbance traveling in the opposite direction. Despite weaknesses in this model, remedied later by Fresnel and others, Huygens was able to apply his principle to prove the laws of both refection and refraction.

Law of Reflection from Huygen's Principle

The figure illustrates Huygen's construction for a narrow, parallel beam of light to prove the law of reflection. Huygen's principle must be modified to accommodate the case in which a wavefront, such as *AC*, encounters a plane interface, such as *XY*, at an angle. Here the angle of incidence of the rays *AD*, *BE*, and *CF* relative to the perpendicular *PD* is θ_i. Since points along the plane wavefront do not arrive at the interface simultaneously, allowance is made for these differences in constructing the wavelets that determine the reflected wavefront.

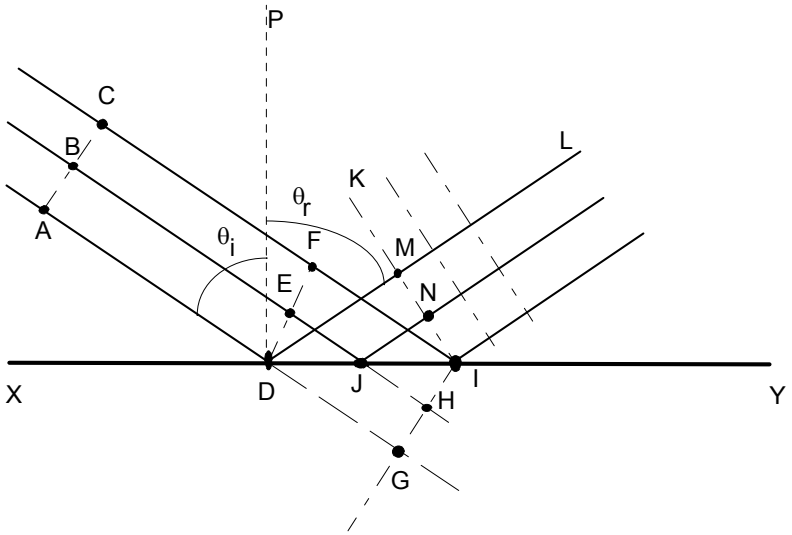

If the interface *XY* were not present, the Huygens construction would produce the wavefront *GI* at the instance ray *CF* reached the interface at *I*. The intrusion of the reflecting surface, however, means that during the same time interval required for ray *CF* to progress from *F* to *I*, ray *BE* has progressed from *E* to *J* and then a distance equivalent to *JH* after reflection. Thus a wavelet of radius *JH* centered at *J* is drawn above the reflecting surface. Similarly, a wavelet of radius *DG* is drawn centered at *D* to represent the propagation after reflection of the lower part of the beam. The new wavefront, which must now be tangent to these wavelets at points *M* and *N*, and include the point *I*, is shown as *KI* in the figure. A representative reflected ray is *DL*, shown perpendicular to the reflected wavefront. The normal *PD* drawn for this ray is used to define angles of incidence and reflection for the beam. The construction clearly shows the equivalence between the angles of incidence and reflection.

Law of Refraction using Huygen's Principle

Similarly, we can use a Huygens construction to illustrate the law of refraction.

Here we must take into account a different speed of light in the upper and lower media. If the speed of light in vacuum is *c*, we express the speed in the upper medium by the ratio c/n_i, where n_i is the refractive index. Similarly, the speed of light in the lower medium is c/n_t. The points *D*, *E* and *F* on the incident wavefront arrive at points *D*, *J* and *I* of the plane interface *XY* at different times. In the absence of the refracting surface, the wavefront *GI* is formed at the instant ray *DF* reaches *I*. During the progress of ray *CF* from *F* to *I* in time *t*, however, the ray *AD* has entered the lower medium, where the speed is different. Thus if the distance *DG* is $v_i t$, a wavelet of radius $v_t t$ is constructed with center at *D*. The radius *DM* can also be expressed as

$$DM = v_t t = v_t\left(\frac{DG}{v_i}\right) = \left(\frac{n_i}{n_t}\right)DG$$

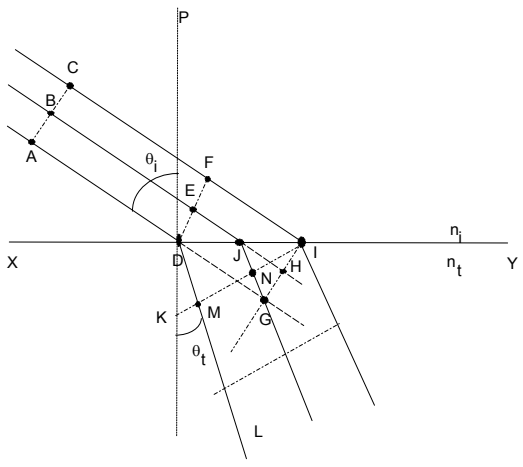

Similarly, a wavelet of radius $(n_i/n_t)JH$ is drawn centered at J. The new wavefront KI includes point I on the interface and is tangent to the two wavelets at points M and N. The geometric relationship between the angles θ_i and θ_t, formed by the representative incident ray AD and refracted ray DL, is **Snell's law**, which may be expressed as

$$n_i \sin\theta_i = n_t \sin\theta_t \quad (1)$$

Fermat's Principle

The laws of geometrical optics can also be derived from a different fundamental hypothesis. Let us suppose that nature is economical, and thus requires that the time required for light to travel from point A to B is the minimum time required. To prove the law of reflection, we use the fact that, for propagation in the same medium, the velocity is a constant and this minimizing the time is the same as minimizing the distance traveled. Consider the following drawing.

Three possible paths from A to B are shown. Let's look at the arbitrary path ACB. If point A' is constructed on the perpendicular AO such that $AO=A'O$, the right triangles AOC and $A'OC$ are equal. Thus $AC=A'C$ and the distance traveled by the ray of light from A to B via C is the same distance from A' to B via C. The shortest distance from A' to B is obviously the straight line $A'DB$, so the path ADB is the correct choice taken by the actual light ray. Geometry shows that for this path, $\theta_i=\theta_r$. Also note that to maintain $A'DB$ as a single straight line, the reflected ray must remain within the plane of incidence.

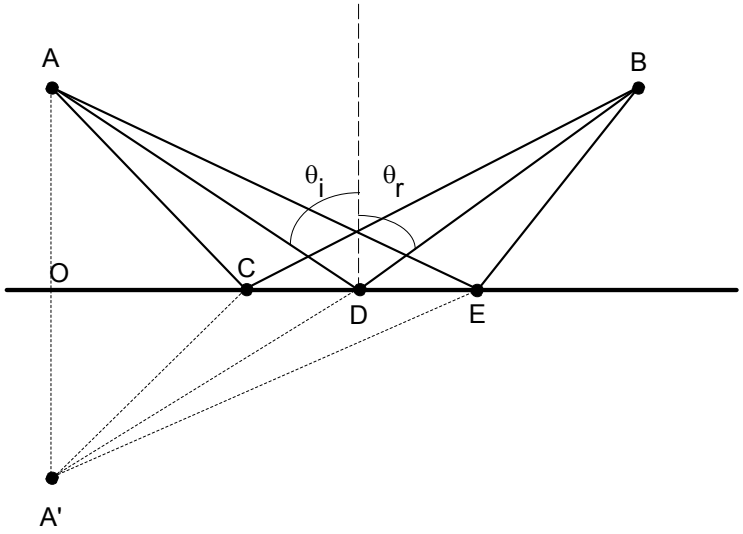

We can also prove the law of refraction. If the light travels more slowly in the second medium, light bends at the interface so as to take a path that favors a shorter time in the second medium, thereby minimizing the overall transit time from A to B.

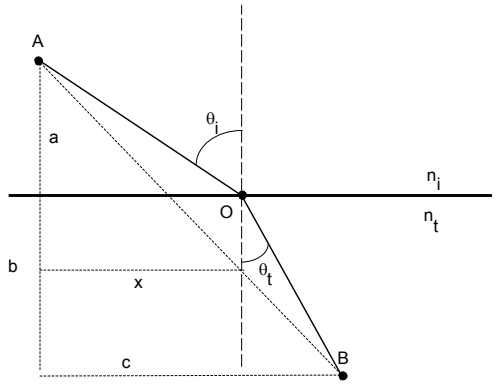

Mathematically, we are required to minimize the total time

$$t = \frac{AO}{v_i} + \frac{OB}{v_t} = \frac{\sqrt{a^2+x^2}}{v_i} + \frac{\sqrt{b^2+(c-x)^2}}{v_t} \quad (2)$$

Since other choices of path change the position of the point O and therefore the distance x, we can minimize the time by setting $dt/dx=0$:

$$0 = \frac{dt}{dx} = \frac{x}{v_i\sqrt{a^2+x^2}} - \frac{c-x}{v_t\sqrt{b^2+(c-x)^2}} = \frac{\sin\theta_i}{v_i} - \frac{\sin\theta_t}{v_t} \quad (3)$$

where the last step used the relationships shown in the figure. Introducing the refractive indices of the media, we arrive at Snell's law

$$n_i \sin\theta_i = n_t \sin\theta_t \quad (4)$$

ISSN 1999-656X

Fermat's principle, like that of Huygens, required refinement to achieve more general applicability. Situations exist where the actual path taken by a light ray may represent a maximum time or even one of many possible paths, all requiring equal time. As an example of the latter case, consider light propagating from one focus to the other inside an ellipsoidal mirror, along any of an infinite number of possible paths. Since the ellipse is the locus of all points whose combined distances from the two foci remain constant, all paths are indeed of equal time. A more precise statement of Fermat's principle, which requires merely an extremum relative to neighboring paths, may be given as follows: **The actual path taken by a light ray in its propagation between two given points in an optical system is such as to make its optical path equal, in the first approximation, to other paths closely adjacent to the actual one**.

With this formulation, Fermat's principle falls in the class of problems called variational calculus, a technique which determines the form of a function that minimizes a definite integral. In optics, the definite integral is the integral of the time required for the transit of a light ray from starting to finishing points.

Optical Path Length

Suppose that we have a stratified material composed of m layers, each having a different index of refraction. The transit time across the layers will then be

$$t = \frac{s_1}{v_1} + \frac{s_2}{v_2} + \cdots + \frac{s_m}{v_m} = \sum_{i=1}^{m} \frac{s_i}{v_i} = \frac{1}{c}\sum_{i=1}^{m} n_i s_i \qquad (5)$$

where the summation is called the **optical path length** traversed by the ray. Clearly for an inhomogeneous medium where n is a function of position, the summation must be changed to an integral

$$(OPL) = \int n(s)ds$$

Since the optical path length is related to the time, we can restate Fermat's principle again as **a light ray in going from point *A* to point *B* must traverse an optical path length that is stationary with respect to variations of that path**.

Optical Reversibility

Consider applying Fermat's principle to an optical system. Since the time must be minimized, we see that the same path is predicted regardless of whether we start at A and travel to B, or start at B and travel to A. In general, any actual ray of light in an optical system, if reversed in direction, will retrace the same path backward. Before discussing the formation of images in a general way, let's look at the simplest - and experimentally, the most accessible - case of images formed by plane mirrors. In this context it is important to distinguish between **specular reflection** from a perfectly smooth surface and **diffuse reflection** from a granular or rough surface. Specular reflection occurs when all the rays of a parallel beam incident on the surface obey the law of reflection from a plane surface and therefore reflect as a parallel beam. In the case of diffuse reflection, although the law of reflection holds locally, the microscopically granular surface results in reflected rays in various directions and thus a diffuse scattering of the originally parallel rays of light. Every plane surface will produce some such scattering, since a perfectly smooth surface is not obtainable in reality. In many cases, however, the diffuse scattering is small and we can approximate the reflection as specular reflection.

Consider the specular reflection of a single light ray from the x-y plane. By the law of reflection, the reflected ray remains within the plane of incidence, making equal angles with the normal at the point of contact. If the path is resolved into components, it is clear that the direction of the incident ray is altered only by reflection along the z direction, and then in such a way that its z component is simply reversed. If the direction of the incident ray is described by its unit vector $\hat{r}_1 = (x, y, z)$, then the reflection causes

$$\hat{r}_1 = (x, y, z) \rightarrow \hat{r}_2(x, y, -z) \qquad (6)$$

It follows that if a ray is incident from such a direction as to reflect sequentially from all three coordinate planes, then

$$\hat{r}_1 = (x, y, z) \rightarrow \hat{r}_2(-x, -y, -z) \qquad (7)$$

and the ray returns precisely parallel to the line of its original approach. A network of such corner reflectors ensures the exact return of a beam of light.

Spectroscopic Photoluminescence of Quantum Dots for Cancer Biomarker Panels

Lina Zhukov
Michael Dybiec
Sergey Ostapenko
Natalia Korsunska

Institute of Semiconductor Physics, National Academy of Sciences, Kiev, Ukraine

Ovarian cancer is the most lethal gynecologic malignancy. This largely reflects the fact that approximately 75% of cases are detected at advanced stages of disease, when cure is unlikely. It is accepted that detecting a greater number of patients with early stage disease by improving screening modalities could significantly improve overall survival. A novel approach to increase the sensitivity and specificity of early detection of cancer is through the application of nanotechnology, where luminescent semiconductor quantum dots (QDs) are conjugated with biomolecules. We report on the luminescence characterization of the bio-conjugated QDs with CA125 antigen using linkage molecules. Kinetic curves of the bio-conjugated 655nm QD luminescence show both photo-enhancement and photo-degradation. Photo-enhancement is measured at various laser density power, temperatures and laser wavelengths. The mechanism of the PL enhancement is discussed.

Keywords: *Spectroscopy, Photoluminescence, Quantum dots, Cancer Biomarker Panels*
Received: 26 August 2009, **Revised**: 17 September 2009, **Accepted**: 22 September 2009

1. Introduction

Ovarian cancer causes more deaths each year among North American women than any other gynecologic cancer. The poor survival rates are largely a reflection of the fact that over 70% of patients are diagnosed with advanced (stage III/IV) disease when 5-year survival rates are less than 20%. This contrasts dramatically with the 80-90% 5-year survival rates associated with patients diagnosed with Stage I or II ovarian cancer. Unfortunately, no good screening tests for ovarian cancer are available. Given our limited understanding of the pathogenesis of epithelial ovarian cancer and consequent difficulty in identifying women at high-risk for development of the disease, there is a great need to establish and translate novel strategies for early detection. Recent discoveries in the molecular biology and molecular genetics of ovarian cancer coupled with technological development in the area of nanotechnology afford an unparalleled opportunity to make radical advances in this arena.

To date, detection of the secreted tumor marker CA 125 is the only biomarker available for screening and therapeutic monitoring, however it has limited sensitivity (70%). A novel approach to increase the sensitivity and specificity of early detection of cancer is through the application of nanotechnology, where luminescent semiconductor quantum dots (QDs) are conjugated with biomolecules [2]. Bioconjugation of QDs, i.e. the attachment of specific ligands to them, represents the convolution of biotechnology and nanotechnology yielding hybrid materials, processes and devices. In a case of early cancer detection this approach offers the potential to detect molecules in biological samples at levels below 10^{-7} [3]. We conjugated in this work core-shell CdSe/ZnS luminescence QDs with monoclonal mouse anti- CA 125 antibody (AB) as a potential serologic assay. Among different monoclonal antibodies potentially available for CA125 detection, we have selected OC-125 for QD-bioconjugation because it recognizes the defined peptide epitope of the target and can be compared with accepted clinical assays.

Nanometer-scale II-VI compound semiconductors known also as quantum dots (QDs) represent zero-dimensional structures where exciton wave function is confined in three

dimensions. This QD's property creates unique optical charcateristics such as spectral tunable photoluminescence (PL) output with external quantum efficiency in the range of 30 to 50% in surface passivated core-shell compounds [1]. Recent improvements in the synthesis of core-shell QDs with the polymer coating show a promise of their wide applications as bio-luminescence markers [2,3]. Tunable wavelength emission of the luminescence QDs was achieved from a variety of the inorganic semiconductors, predominantly of II-VI compounds such as CdSe, CdTe, CdS, etc. To obtain a noticeable quantum efficiency of the QD luminescence the core-shell structures can be effectively designed in a form of colloidal particles. A successful example represents CdSe/ZnS core/shell coupling, where large band-gap material (ZnS) serve as a surface passivating layer and as a barrier assisting the electron-hole confinement in the CdSe core [4]. A stability and efficiency of the QD luminescence is a critical aspect.

2. PL System

The PL spectroscopy was performed between 80K and room temperature, using a 50mW HeCd laser line at 325 nm or 200mW Ar^+ laser line at 488 nm as the excitation sources. Laser power density varied by use of a set of calibrated neutral density filters and could be focused down to 100 microns spot. At low intensity measurements the laser beam was un-focused with approximately 1.5mm laser spot diameter at the sample surface. The PL signal was collected by optics, dispersed by a SPEX 500M spectrometer and recorded by a photo multiplier tube coupled with a lock-in amplifier. All system is computer controlled.

3. Anitigen Detection

CA 125 assay was determined by using the OC 125 mouse monoclonal antibody (Mab) (DAKO Cytomation, Carpinteria, CA), as the detector antibody. These Mabs were produced using lymphocytes from a mouse immunized with OVCA 433, a cell line derived from a papillary serous cystadenocarcinoma of the ovary [4]. We also utilized a biotinylated capture antibody, designated as anti-epithelial ovarian carcinomas (Biomeda, San Francisco, CA). This binds mucin-like glycoprotein molecules containing OC 125 defined antigen, similar to mouse monoclonal M1 1 clone [5].

The samples, standards and controls and biotinylated capture antibody were incubated in the microtiter streptavidin-coated black plates from Thermo Electron (Milford, MA). The OC 125 mouse Mabs were pre-labeled with QDs 655 goat-F(ab')2 anti-mouse IgG conjugate before applying to the bound (captured) antigen in the solid phase well. The molar ratio 6:1 of Fab-QDs 655 to labeled antibody molecule was found sufficient to get strong PL signal from the labeled complex. These experimental findings are consistent with our previous experience in the application of alternative Zenon antibody labeling method for lung cancer biomarkers evaluation [6], in which specific antibodies were directly labeled with isotype specific Fab fragments conjugated with Alexa Fluor dyes (Molecular Probes, Eugene, OR). Following incubation time with QDs- pre-labeled antibodies and washing steps the plates were read according to emission spectra for the tested QD-bioconjugate (see spectra below).

We used as a reference standard the serial dilution of human CA 125 antigen of high purity grade (Research Diagnostics, Inc., Flanders, NJ). Control wells either lacked antigen or contained QDs 655-Fab only (without antibody). The plasma samples from cancer patients were assayed using the reference ELISA kit for measurement of CA125 (Biomeda). The reportable (dynamic) range of CA125 detectable by the Biomeda assay is 0 to 500U/ml, which reflects the physiological range of CA125 in blood. These standards were used to generate a calibration curve, which is depicted as the fitted line (in red) in Fig. (1). Two blood samples with the lowest and highest CA125 levels (blue dots) were then assayed using PL method, in which OC 125 mouse Mab was labeled with QDs 655 (described above). These results show strong concordance of QD 655 assay with reference CA 125 measurement.

4. Results and Discussion

Commercially available CdSe/ZnS polymer coated quantum dots from Quantum Dot Corp**.** were used [8]. A sample of the Qdot 655 Goat $F(ab')_2$ anti-Mouse IgG conjugate in a form of a mm-size spot was dried on a polished surface of the crystalline silicon substrate to achieve low level of the scattered light. One dried spot contained 2µl of QD's bio-conjugate diluted with phosphate buffer (PBS) in the 1:50 volume ratio. Bio-conjugated samples contained Qdot 655 $F(ab')_2$ complex fragment conjugated to OC125 detector antibody that recognizes CA125 anti-gene molecule, used in early stage detection of ovarian cancer. Some experiments were done on QD – $F(ab')_2$ – OC125 bio-conjugate structure before attachment to CA125 anti-gene molecule.

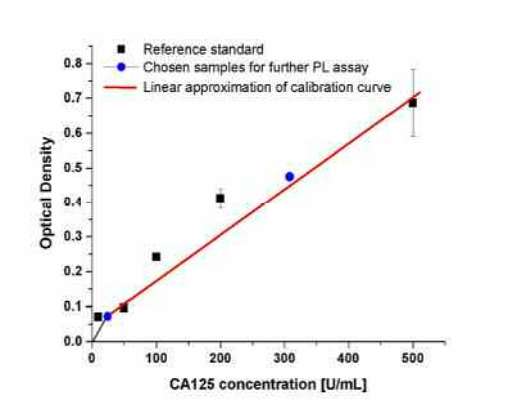

Fig. (1) Concentration of CA125 (U/ml) in cancer plasma samples in the PL study measured using standard ELISA methodology

(a) Photoluminescence transient [7]

PL spectrum of the CdSe/ZnS quantum dots in the range of 0.73 to 3.54 eV (350 to 1,700 nm) exhibits only one prominent luminescent band with the maximum at 1.89eV (655 nm) and half-width of 0.09eV at room temperature (Fig. 2).

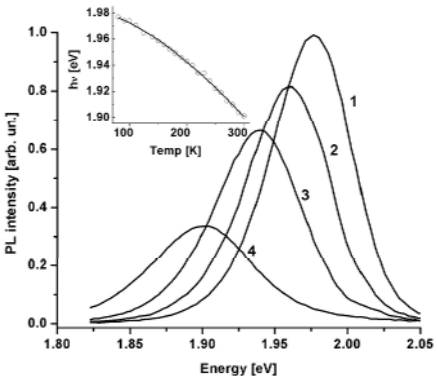

Fig. (2) PL spectrum of the CdSe/ZnS quantum dots in the range of 0.73 to 3.54eV (350 to 1700nm)

When temperature is decreased the PL maximum shows a narrowing and "blue" shift following the temperature band-gap variation of the bulk CdSe, which is described in Fig. (1) by a solid line using Varshni equation.

The following observations were depicted based on the transient PL study.

(1) PL photo-enhancement amplitude can be quite substantial spanning the range from 10% up to 5-fold with respect to the initial luminescence intensity.

(2) The enhancement effect is observed both at 325nm (HeCd) or 488nm (Ar^+) laser excitation. The enhancement rate is increased (time constant reduced) at higher excitation power density as illustrated in (Fig. 3).

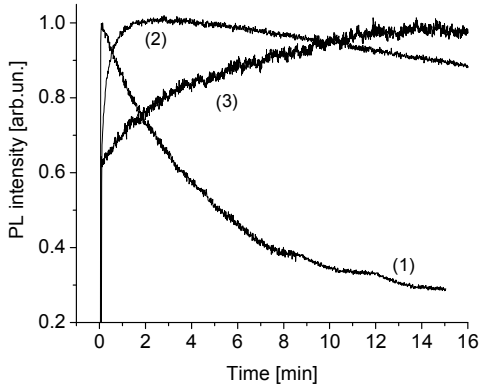

Fig. (3) The enhancement rate is increased (time constant reduced) at higher excitation power density

(3) If the sample subjected to UV exposure was held in dark for definite time, the enhancement effect can be either recovered back which is assigned to reversible enhancement (RE) and the kinetics can be repeated again, or the effect can exhibit non-reversible enhancement (NRE) and show no recovery at room temperatures for at least over night sample storage. Typically RE and NRE occur simultaneously (Fig. 4)

(4) Both RE and NRE kinetics are thermally activated meaning that they are substantially slowed down when temperature decrease. Specifically, the RE time constant (τ_{RE}) yields ten's of minutes at 300K and its transient kinetics is no longer observed below 240K.

(5) The PL spectrum measured at room temperature before and after enhancement completed shows no noticeable variation of the peak position and the half-width.

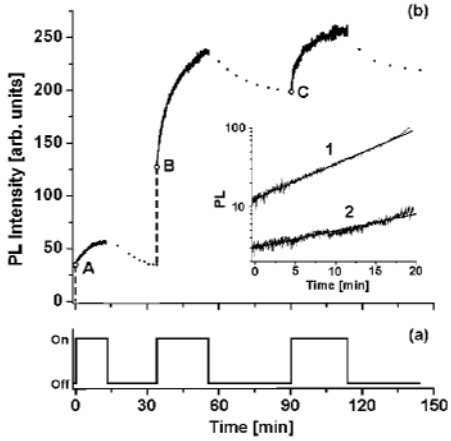

Fig. (4) If the sample subjected to UV exposure was held in dark for definite time, the enhancement effect can be either recovered back which is assigned to reversible enhancement (RE) and the kinetics can be repeated again, or the effect can exhibit non-reversible enhancement (NRE) and show no recovery at room temperatures for at least over night sample storage

(b) Silicon Substrate

With the goal of increasing sensitivity of the screening test for ovarian cancer by detecting low levels of CA 125 and in reducing background to zero over a broad spectral range, a Si substrate was used in place of the commercially available plastics used in standard immunosorbent assay. A Si wafer as a substrate shows negligible scattered signal in a broad visible spectral range from 350 to 725nm, making it ideal for use in quantum dot optical multiplexing. Figure (5) shows the comparison between some common plastics used in ELISA plates compared to Si wafer.

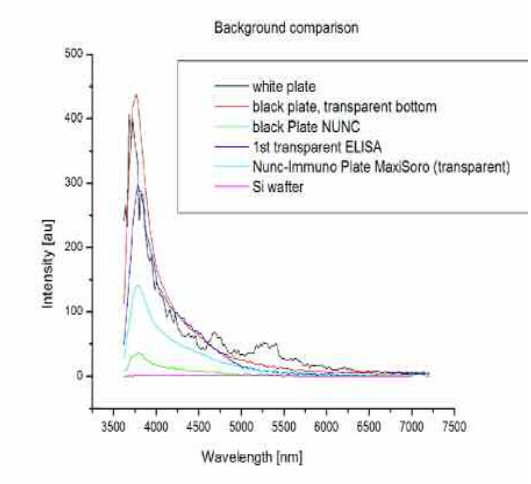

Fig. (5) Comparison between some common plastics used in ELISA plates compared to Si wafer

5. Conclusions

QD luminescence biomarkers are detected within the physiological range in plasma. Application of Quantum Dot bioconjugates allowed us to detect antigens below limits of standard tests used in clinics. The use of Silicon as a substrate instead of plastics allowed to further lower the limit of detection of antigen. It also lays the groundwork for a multiplexed biomarker panel by reducing background noise over the entire area of interest to near zero. It was found that the signal from QD's could be enhanced in a controlled manner by using a low power excitation source for some time before the signal is read.

References

[1] M.A. Hines, P. Guyot-Sionnest, *J. Phys. Chem.*, 100 (1996) 468.

[2] M. Bruchez et al., *Science*, 281(5385) (1998) 2013.

[3] E.R. Goldman et al., *phys. stat. sol. b*, 229 (2002) 407.

[4] R.C. Bast Jr. et al., *Reactivity of a monoclonal antibody with human ovarian carcinoma., J. Clin. Invest.*, 68(5) (1981) 1331.

[5] T.J. O'Brien et al., *New monoclonal antibodies identify the glycoprotein carrying the CA 125 epitope., Amer. J. Obstet. Gynecol.*, 165(6 Pt 1) (1991) 1857-1864.

[6] T.A. Zhukov, J.L. Kroeger and M.S. Tockman, *Lung cancer biomarker evaluation: Comparison of flow cytometry and laser scanning cytrometry in assessment of macrophage migration inhibiroty factor (MIF) expression in lung carcinoma cell lines and sputum specimens.* in *AACR Annual Meeting*. 2004. Orlando, FL.

[7] N.E. Korsunska et al., *Semicond. Sci. Technnol.*, 20(8) (2005) 876-881.

Analytical Equivalent Optical Properties of CdS-Cu_xS Thin Films Deposited on Glass Substrate by Spray Pyrolysis

Violeta Popescu
Horea Iustin Naşcu

Department of Chemistry, Technical University of Cluj-Napoca, Romania

Multi-layered, firmly adherent, optically clear CdS/Cu_xS films were deposited by spray pyrolysis on glass substrate. The glass/CdS/Cu_xS system was investigated. Firstly, CdS films were deposited using a solution containing $CdCl_2$ and thiourea. For Cu_xS films deposition the solution used consisted on $CuCl_2$ and thiourea. Multilayered films were also deposited. Mixed films of copper and cadmium sulfides were also deposited from solutions containing both copper and cadmium salts and thiourea on heated glass substrates, by spray pyrolysis. Visible transmission spectra were recorded for CdS/Cu_xS films. The film characteristics depend on the concentration and the molar ratio of cadmium and copper salts. These thin layers may be applied in solar control coatings, leading to important energy saving for air conditioning devices used for cars or other closed spaces.

Keywords: *Mixed thin films, Cadmium sulfide, Copper sulfide, Spray pyrolysis*
Received: 20 July 2009, **Revised**: 22 September 2009, **Accepted**: 27 September 2009

1. Introduction

Thermo-reflecting thin-films used for solar control should have a transmittance ranged between 10 and 30% for the visible part of light radiation, i.e. in the range 400-700nm (VIS), and near infrared reflection (NIR, 0.7-2.5μm) between 15 and 50 % [1-8]. Metallic sulphides thin-films with termo-reflecting properties can be obtained by chemical route and the most frequently used method according to literature is the chemical bath deposition (CBD) [1-7] followed by spray pyrolysis [10-14] and by other physical methods.

In a previous work, thermo-reflecting thin layers of PbS, CdS, Cu_xS and Au were obtained [9-15]. CuS thin films with the thickness in the range 15-62 nm, - deposited by spray pyrolysis – exhibit a VIS transmission of about 30 – 80% and, simultaneously, a NIR reflection of about 15-25% [13,14]. CdS films deposited in the same way with thickness from 39 to 63 nm presented a transmission of about 50-59.8%, for neutral filter and a NIR reflection from 5% to 30% [11]. In the present paper are reported the results of a study concerning the preparation of mixed CdS-Cu_xS thin layers by spray pyrolysis as well as their optical properties.

2. Experiment

Mixed sulphides thin films were deposited on heated glass substrate by spray pyrolysis from solutions containing cadmium and copper salts, thiourea (TU). In some particular cases, surfactants (polyethyleneglycole – PEG or ethersulphate), were used for higher uniformity of the films [12-14]. CdS-Cu_xS thin films were successfully deposited both as multi-layers (glass|CdS|CuS) and as mixed films. For multi-layers, on the heated glass substrate a layer of CdS was deposited first, and then on the surface of the deposited CdS a layer of CuS was deposited. For mixed CdS+CuS layers, solutions containing both Cd and Cu and a sulphur compound were used. The concentration of reagents and the number of deposited layers have been varied. In a preliminary stage of this work, the optimum flow-rate of spraying solution, the flow-rate of air and the distance between substrate and spraying nozzle have been determined. Furthermore, for these films the transmission in white light were measured by using a FEK-M photo-colorimeter, for λ=600nm – neutral filter - and for λ=540nm – green filter. The VIS transmission spectra were recorded with SPECORD UV-VIS and the reflection spectra with a UR-20 spectrophotometer (Carl-Zeiss, Jena) using usual standards and LiF prism.

ISSN 1999-656X PRINTED IN IRAQ

3. Results and discussion

3.1 Preparation of (Cd-Cu)S mixed films

In order to obtain mixed cadmium and copper sulphides by spray pyrolysis, solutions containing both cadmium and copper salts, thiourea, as source of sulphur, and PEG as surfactant, were used. The reactions that take place during the deposition process were previously reported [10,13,14]. For obtaining (Cd-Cu)S mixed films, spray pyrolysis deposition on heated glass slides was used, maintaining a constant temperature of 400°C. The reaction between cadmium and copper salts with thiourea took place instantly on the heated glass surface. The flow rate of the solution was maintained in the range 20-24 ml/minute.

The deposition solution contains cadmium and copper chlorides and their molar ratio was varied between 1:1 and 4:1. The concentrations of cadmium chloride (5×10^{-2}M) and of thiourea (0.25M) were kept constant but the copper chloride concentration vas variable in the range 1.25×10^{-2}-5×10^{-2}M. The PEG surfactant concentration was maintained at 0.1%. From this solution, two consecutive sulphide layers were deposited, the deposition time being 10 s for each layer. In table (1), the conditions for obtaining these layers are given together with the transmission T%, in white light (neutral filter) and in green light (green filter).

Table (1) Composition of the solutions used for deposition of mixed cadmium and copper sulphides by spray pyrolysis and transmission in films measured after deposition

Sample No.	Concentration				T neutral filter [%]	T green filter [%]	Qualitative remarks
	$CuCl_2x10^2$ [M/L]	$CdCl_2x10^2$ [M/L]	TU [M/L]	PEG [%]			
1	5	5	0.25	-	48	44.2	Optical clear film, yellow-brownish in transmission, yellow-purplish metallic in reflection
2	5	5	0.25	0.1	62	59.8	Macroscopic appearance of the film alike that of film no.1.
3	2.5	5	0.25	0.1	55.8	51	Optical clear film, yellow-brownish
4	1.25	5	0.25	0.1	54.2	49.2	Uniform, optical clear film, yellow-brownish clearer than the precedents.

3.2 Optical properties of thin films

All mixed (Cd-Cu)S thin films presented in table 1 are optically clear, with un appearance similar to that of CdS films. The presence of CuS changed the shade of the film, this exhibiting a brownish tint, with a particular aesthetic aspect. The VIS transmission of the film, measured with a neutral filter ranged in the interval 48 – 62 %, being intermediate between the transmission of pure CuS and CdS layers.

On the other hand, an influence of surfactant presence in the spraying solution may be noticed. Thus, sample 2, deposited in the presence of PEG, in the same conditions as sample 1 and looking very similar, exhibits a higher transmission both for neutral and green filter. It is well known that the surfactant presence in the solution leads to the obtaining of lower grain size for particles in the film. This fact has an evident influence on the optical properties of thin films obtained.

VIS transmission spectra of (Cd-Cu)S thin films, with the compensation of substrate effect, were recorded (Fig. 1). As seen from Fig. 1 the transmission of (Cd-Cu)S layers was intermediate between the transmissions of individual CdS and CuS layers. Since the transmission for wavelengths higher than 500nm is greater than 60 % for all samples, this film is potentially useful for obtaining thermo-reflecting layers.

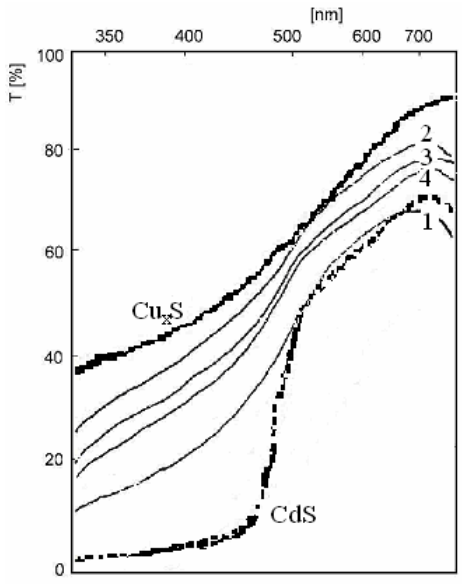

Fig. (1) Optical visible transmission spectra for CdS-Cu_xS mixed films (samples from table 1)

By selecting proper deposition conditions, thin films with different optical properties are obtained. The NIR reflection spectrum only for the most uniform sample (sample 4) was recorded. Different aspects of the reflection spectra are noticeable. A flat peak for wavelengths higher than 0.2μm appears, as compared to the reflection spectra of pure CdS or Cu_xC. The reflectance diminishes abruptly for wavelengths lower than 2.8μm (Fig. 2).

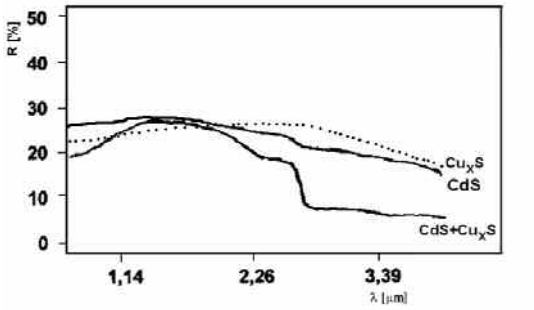

Fig. (2) NIR reflection spectra of some a mixed film of CdS and Cu_xS compared with pure CdS and Cu_xS films

3.2 Deposition of multilayer films

In the preparation of both multilayer thin films and the mixed films, as presented above, our goal was to improve the optical characteristics of these films as compared to each individual sulphide. The optimum deposition conditions for every sulphide were published elsewhere [9-14]. Thin films of CdS were deposited from equimolar cadmium chloride and thiourea 0.1M solutions. The range of concentration for solutions used in obtaining CuS thin films fall between 8.3×10^{-2}–1.67×10^{-2}M for $CuCl_2$ and between 8.3×10^{-2}–8.3×10^{-1}M for thiourea. Cetyl-pyridinium bromide (CPB) - $C_{21}H_{38}NBr$ (cationic surfactant), and polyethyleneglicole (PEG-600) were used as surfactants.

Multilayer films with the structure glass |CdS|Cu_xS have been deposited. This type of layers consists of 1-3 layers of CdS and layers of Cu_xS. Optically clear sandwich type layers with a brown-yellow colour in transmission and in the same time purplish in reflection with a VIS transmission in the boundary of 35 – 58 % have been obtained.

When higher concentration was used for the precursor solutions, 0.167M $CuCl_2$, 0.83M thiourea and equimolar 0.1M $CdCl_2$ – thiourea respectively, by applying 3 layers of each sulphide type, distinct color nuances on the two sides of glass slides could be obtained. For instance a pair of colours was purplish-yellow and metallic grey. In the later case the transmission was 24-26.5 % for visible light.

The optimum condition for obtaining an optical clear CdS/Cu_xS thin film with a transmission of about 45% and a purplish-metallic reflection, almost identical on both sides are: consecutive deposition of three CdS layers for 10 seconds each, from a solution with the composition: 0.1M $CdCl_2$, 0.1M thiourea, 0.1% PEG-600 at 450°C followed by deposition of three Cu_xS layers from other solution: 1.67×10^{-2}M $CuCl_2$, 8.3×10^{-2}M thiourea and 1.67×10^{-2}% CPB.

Optically clear thin films with a transmission of 24-58% and a brown-orange aspect in transmission but other different nuances in reflection on both sides (purplish-yellow and metallic grey) have been obtained in the conditions described above.

3.3 VIS transmission of multilayer films

In Fig. (3) VIS transmission spectra for the representative sample of CuS/CdS are shown. The transmission for wavelengths higher than 500 nm is smaller than 60 % for samples 7 and 8. The Cu_xS film presented in Fig. (3) was obtained by the deposition of 3 layers from a solution containing 0.01M $CuCl_2$, 0.01M TU, 10^{-2} % CPB [12]. For comparison the spectra of a CdS film is also presented. The 3-layered CdS film was obtained from a solution containing 0.075M $CdCl_2$, 0.1M thiourea; 3×10^{-3} % ether sulphate [11].

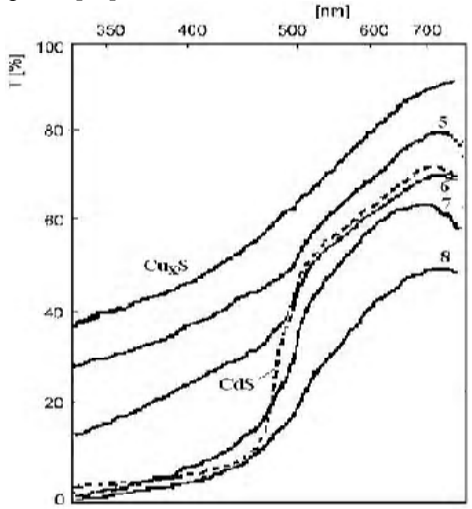

Fig. (3) Optical visible transmission spectra for multilayered Cu_xS/CdS films (samples from table 2)

It may be seen that the spectra for samples 7 and 8 has a shape rather similar to that of CdS films but presents a lower transmission, for wavelengths over 480nm. The outstanding aesthetic appearance is an important quality for their potential application on glass panels used in modern architecture and in manufacturing of glasses for automotive industry. We believe also that practical application of these films may be extended in manufacturing of photovoltaic cells [16-19]. By varying the deposition conditions,

thin films with different properties could be obtained and thus, by selecting the deposition parameters, the optical properties of the film can be controlled.

4. Conclusion

The optimal conditions for preparing mixed and multilayer cadmium and copper sulphide thin films by spray pyrolysis were established. The mixed CdS-CuS thin films obtained in this paper present a good VIS transmission (26-52%). By varying the composition of the deposition solutions and the number of applied layers, thin films with outstanding aesthetic appearance and various optical properties could be obtained. These thin layers may be applied in solar control coatings, leading to the achievement of important energy saving for air conditioning devices used for cars or other closed spaces.

References

[1] P.K. Nair, M.T.S. Nair, A. Fernandez, M. Ocampo, *J. Phys. D. Appl. Phys.*, 22 (1989) 829.
[2] P.K. Nair, M.T.S. Nair, *Semicond. Sci. Technol.*, 4 (1989) 807.
[3] P.K. Nair, M.T.S. Nair, *J. Phys. D. Appl. Phys.*, 23(2) (1990) 150.
[4] P.K. Nair, M. Ocampo, A. Fernandez, M.T.S. Nair, *Solar Energy Mater.*, 20(3) (1990) 235.
[5] C. Naşcu et al., *Chem. Quarterly Rev.*, 5(3) (1997) 201.
[6] C. Naşcu, I. Pop, V. Ionescu, *Revista de Chimie* (in French), 48(8) (1997) 696.
[7] I. Pop et al., *Thin Solid Films*, 307(1-2) (1997) 240.
[8] K. Vergupalan et al., *Bull. Electrochem.*, 10 (11-12) (1994) 504.
[9] H. Naşcu et al., *Int. Conf. on Mater. Sci. and Engineering*, Braşov (2001) BRAMAT, vol. IV, 31.
[10] V. Popescu and H.I. Naşcu, *Studia Univ. Babeş-Bolyai, Chemia, XLVI*, 1-2 (2001) 143.
[11] V. Popescu, R.Grecu and E.M. Pică, *Studia Univ. Babeş-Bolyai, Chemia*, XLVI, 1-2 (2001) 149.
[12] V. Popescu, *Proc. Int. Conf. on Mater. Sci. and Eng.*, BRAMAT, 13-14 March, Braşov, 2003, vol. IV, Braşov, 67.
[13] C. Naşcu et al., *Mater. Lett.*, 32 (1997) 73.
[14] H. Naşcu and V. Popescu, *Proc. Int. Conf. on Mater. Sci. and Eng.*, BRAMAT, 13-14 March, Braşov, 2003, vol. IV, 61.
[15] V. Popescu, I. Bratu, H.I. Naşcu, *Acta Technica Napocensis*, 42 (1999) 187.
[16] A.M. Al-Dhafiri et al., *J. Cryst. Growth*, 86(1-4) (1990) 900.
[17] S. Oktik, G.J. Russell and J. Woods, *J. Cryst. Growth*, 59(1-2) (1982) 414.
[18] N.B. Chaure et al., *Thin Solid Films*, 437(1-2) (2003) 10.
[19] J. Herrero et al., *Thin Solid Films*, 361-362(21) (2000) 28.

2009 Physics Nobel Prize
Kao, Boyle & Smith

The Iraqi Journal of Applied Physics is proud to present a brief on this year's Nobel Laureates in Physics, Drs. Willard Boyle and George Smith, formerly of Bell Labs, for their invention of the charge-coupled device; and Dr. Charles Kao, of Standard Telecommunication Laboratories, Harlow, UK, and Chinese University of Hong Kong, for his work in development of optical fibers for telecommunications.

The part of this year's award associated with Mr. Kao underscores the fact that optical fibers carry an increasing fraction of phone calls, television programs, and internet traffic into homes. Data can move down silicon fiber more quickly than through copper wire because nothing is faster than light, and light signaling offers higher bandwidth for electronic circuitry. Encoding information in the form of light pulses rather than as electric pulses allows more data to flow down a line. Kao's principal achievement was in making the fiber more efficient; by excluding impurities in the fiber material, he developed a material that absorbed less of the light carrying signals over long distances.

The part of the prize associated with Boyle and Smith recognizes the huge advantage of capturing images in digital rather than film form. Pictures can be sent through wires more easily, can be manipulated and processed in creative ways (e.g., you can see a moving comet or supernova in sky scans by subtracting tonight's pixel map from last night's map), and can be stored more handily. Devices such as photomultiplier tubes for converting light into an electric signal have been around for decades. But the CCD allowed whole two-dimensional fields of optical data to be read out more quickly and efficiently. And, of course, CCD's have been the backbone of the commercial digital camera industry.


Charles Kao


Willard Boyle


George Smith

Overview of optical fibers and charge-coupled devices

THE 2009 NOBEL PRIZE IN PHYSICS will be awarded to **Charles K. Kao** (Standard Telecommunication Laboratories, Harlow, UK, and Chinese University of Hong Kong), and **Willard S. Boyle** and **George E. Smith** (both of whom worked chiefly at Bell Laboratories, in Murray Hill, NJ, USA) for their work leading to modern telecommunications. Kao will receive half the prize money for helping to invent modern optical fiber, allowing signals to travel flawlessly thousands of miles. Boyle and Smith will split the other half of the prize for their development of charge coupled devices (CCDs).

"The [transfer of] information in society today is completely based on [this research]," said Joseph Nordgren, the chair of the Nobel Prize committee in a press conference announcing the prize. "The practical implications for this research were enormous...It is something that has changed our life, not just in science but in society as whole."

Fred Dylla, CEO of the American Institute of Physics, which publishes *Physics Today*, concurs. "When combined with the laser and the transistor, the invention of an efficient, low-loss optical fiber has made nearly instantaneous communication possible across the entire globe. This mode of communication is essential for high-speed internet and forms the optical backbone of 21st century commerce. The CCD sensor has revolutionized technical, professional, and consumer photography in the last few decades. Taken together these inventions may have had a greater impact on humanity than any others in the last half century."

"Optics technologies are exceptionally significant for scientific developments in today's world," said Elizabeth Rogan, CEO, of the Optical Society of America. "We congratulate Kao, Boyle and Smith on this much-deserved recognition."

Kao

In 1966, Charles K. Kao made a discovery that led to a breakthrough in fiber optics. He carefully calculated how to transmit light over long distances via optical glass fibers. With a fiber of purest glass it would be possible to transmit light signals over 100 kilometers, compared to only 20 meters for the fibers available in the 1960s. "It was the impurities, and other limiting factors such as scattering, atomic motion, that limited glass fibers in the 1960s," said Nordgren.

Kao presented his research at the 1966 London meeting of the Institution of Electrical Engineers. The first ultrapure fiber was successfully fabricated just four years later, in 1970 by the Corning company.

"The Nobel Prize isn't awarded for lifetime achievement, it is given for diverse research, clearly Kao's work achieved a breakthrough that led to a whole new research and technology field," said Nordgren.

Boyle and Smith

In 1969 Willard S. Boyle and George E. Smith invented the first successful imaging technology using a digital sensor, a CCD (charge-coupled device).

The two researchers came up with the idea in just an hour of brainstorming, according to Boyle who spoke during a press conference today. "It is amazing that a [the CCD device] was created so quickly," said Nordgren. "There are so many breakthroughs that came out of research at Bell labs...it's unfortunate that during the 80s, US companies abandoned the idea of having a scientific environment such as Bell labs," said Nordgren.

Boyle said that to him, the biggest achievement of his work was seeing images transmitted back from Mars. "It wouldn't have been possible without our invention," he said.

The CCD technology makes use of the photoelectric effect, as theorized by Albert Einstein and for which he was awarded the 1921 Nobel Prize. By this effect, light is transformed into electric signals. The challenge, when designing an image sensor, was to gather and read out the signals in a large number of image points, pixels, in a short time.

The CCD is the digital camera's electronic eye. It revolutionized how images were collected from spacecraft, by telescopes, and in medical imaging, and has eventually replaced the film camera in every aspect of photography.

Edited by
Oday A. Hamadi
Managing Editor, IJAP

ISSN 1999-656X

PRINTED IN IRAQ

IRAQI JOURNAL OF APPLIED PHYSICS LETTERS

CONTENTS